Heliyon 10 (2024) e28645

Contents lists available at ScienceDirect

Heliyon

journal homepage: www.cell.com/heliyon

Research article

Integrated analysis of m6A regulator-mediated RNA methylation modification patterns and immune characteristics in Sjögren's syndrome

Junhao Yin [a,b,c,d,1], Jiayao Fu [a,b,c,d,1], Jiabao Xu [a,b,c,d], Changyu Chen [a,b,c,d], Hanyi Zhu [a,b,c,d], Baoli Wang [a,d], Chuangqi Yu [a,d], Xiujuan Yang [a,d], Ruiyu Cai [e], Mengyang Li [e], Kaihan Ji [e], Wanning Wu [e], Yijie Zhao [f], Zhanglong Zheng [g], Yiping Pu [a,b,c,d,*], Lingyan Zheng [a,b,c,d,**]

[a] *Department of Oral Surgery, Shanghai Ninth People's Hospital, Shanghai Jiao Tong University School of Medicine, College of stomatology, Shanghai Jiao Tong University, Shanghai, China*
[b] *National Center for Stomatology & National Clinical Research Center for Oral Disease, Shanghai, China*
[c] *Shanghai Key Laboratory of Stomatology, Shanghai, China*
[d] *Shanghai Institute of Stomatology, Shanghai, China*
[e] *College of Stomatology, Shanghai Jiao Tong University, Shanghai, China*
[f] *Department of Oral and Maxillofacial Surgery, Shanghai Stomatological Hospital, Fudan University, 1258 Fuxin Zhong Road, Shanghai 200031, China*
[g] *Department of Oral and Maxillofacial Surgery, School and Hospital of Stomatology, Tongji University, Shanghai Engineering Research Center of Tooth Restoration and Regeneration, Shanghai, China*

ARTICLE INFO

Keywords:
Sjögren's syndrome
Epigenetics
Immune characteristics
machine learning
Random forest

ABSTRACT

The epigenetic modifier N6-methyladenosine (m6A), recognized as the most prevalent internal modification in messenger RNA (mRNA), has recently emerged as a pivotal player in immune regulation. Its dysregulation has been implicated in the pathogenesis of various autoimmune conditions. However, the implications of m6A modification within the immune microenvironment of Sjögren's syndrome (SS), a chronic autoimmune disorder characterized by exocrine gland dysfunction, remain unexplored. Herein, we leverage an integrative analysis combining public database resources and novel sequencing data to investigate the expression profiles of m6A regulatory genes in SS. Our cohort comprised 220 patients diagnosed with SS and 62 healthy individuals, enabling a comprehensive evaluation of peripheral blood at the transcriptomic level. We report a significant association between SS and altered expression of key m6A regulators, with these changes closely tied to the activation of $CD4^+$ T cells. Employing a random forest (RF) algorithm, we identified crucial genes contributing to the disease phenotype, which facilitated the development of a robust diagnostic model via multivariate logistic regression analysis. Further, unsupervised clustering revealed two distinct m6A modification patterns, which were significantly associated with variations in immunocyte infiltration, immune response activity, and

* Corresponding author. Department of Oral Surgery, Shanghai Ninth People's Hospital, Shanghai Jiao Tong University School of Medicine, College of stomatology, Shanghai Jiao Tong University, Shanghai, China.
** Corresponding author. Department of Oral Surgery, Shanghai Ninth People's Hospital, Shanghai Jiao Tong University School of Medicine, College of stomatology, Shanghai Jiao Tong University, Shanghai, China.
E-mail addresses: yvettepeen@126.com (Y. Pu), zhenglingyan73@163.com (L. Zheng).
[1] These authors contribute equally to this work.

https://doi.org/10.1016/j.heliyon.2024.e28645
Received 23 January 2023; Received in revised form 17 March 2024; Accepted 21 March 2024
Available online 29 March 2024

biological function enrichment in SS. Subsequently, we proceeded with a screening process aimed at identifying genes that were differentially expressed (DEGs) between the two groups distinguished by m6A modification. Leveraging these DEGs, we employed weight gene co-expression network analysis (WGCNA) to uncover sets of genes that exhibited strong co-variance and hub genes that were closely linked to m6A modification. Through rigorous analysis, we identified three critical m6A regulators - *METTL3*, *ALKBH5*, and *YTHDF1* - alongside two m6A-related hub genes, *COMMD8* and *SRP9*. These elements collectively underscore a complex but discernible pattern of m6A modification that appears to be integrally linked with SS's pathogenesis. Our findings not only illuminate the significant correlation between m6A modification and the immune microenvironment in SS but also lay the groundwork for a deeper understanding of m6A regulatory mechanisms. More importantly, the identification of these key regulators and hub genes opens new avenues for the diagnosis and treatment of SS, presenting potential targets for therapeutic intervention.

1. Introduction

Sjögren's syndrome (SS) is a classical autoimmune disorder with an estimated prevalence of 0.5%–1% [1]. It is distinguished by localized inflammation that culminates in the dysfunction of salivary and lacrimal glands, disrupting normal secretion processes [2,3]. However, the clinical manifestations of SS transcend secretory organ impairment, extending to parenchymal organs including the kidneys, lungs, and liver. This expansive impact is likely due to periepithelial infiltrates observed within these organs [4]. SS unfolds across three principal stages, each delineating a progressive escalation in disease complexity. Initially, the disease is marked by the demise of acinar epithelial cells. The subsequent stage witnesses an accumulation of immune cells, starting with macrophages and dendritic cells, and soon involving $CD4^+$ T cells and $B220^+$ B lymphocytes, coupled with autoantibody production. The final stage is characterized by the emergence of pronounced clinical symptoms. It is during the intermediate to late stages of SS that abnormal humoral immune responses become prominent, chiefly driven by autoreactive B cells. These cells are identifiable by markers such as anti-ds-DNA, anti-nuclear antibodies, rheumatoid factor, and anti-Ro/SSA and anti-La/SSB antibodies, illustrating the multifaceted immune dysregulation inherent to SS progression. These humoral immune responses are mainly regulated by $CD27^+$ memory B cells and terminally differentiated plasma cells. Additionally, chemokines such as CXCR3, CXCR4, CXCL12, and CXCL13 play a role, contributing to the extensive infiltration of autoreactive B cells in salivary gland lesions and the formation of ectopic germinal centers. Observations indicate that SS patients exhibiting germinal center-like structures in labial gland biopsies face an increased risk of developing non-Hodgkin's lymphoma, alongside elevated mortality rates [5,6]. Therefore, enhancing our comprehension of immune regulation in SS is pivotal for identifying underlying pathological mechanisms. Such insights could pave the way for the development of targeted immuno-based therapeutic strategies, offering hope for improved patient outcomes.

The m6A modification was first discovered in 1974 and is the most common RNA epigenetic modification in eukaryotic cells [7,8]. Research has revealed RNA methylation to be a dynamic and reversible process that can influence RNA behavior—encompassing transcription, splicing, degradation, and translation—without altering the base sequence. This epigenetic control mechanism is implicated in the development of several diseases, including systemic lupus erythematosus [9], rheumatoid arthritis [10], and autoimmune thyroid disease [11], by modulating gene expression pathways and disease progression. Regulators of this methylation modification include methyltransferases, demethylases, and methylation readers [12]. The m6A methyltransferase complex, comprising multiple components including METTL3, METTL14, and WTAP, primarily catalyzes the m6A modification of adenine residues on RNA, playing a pivotal role in post-transcriptional regulation. Demethylases, such as FTO and ALKBH5, serve to remove m6A modifications from nucleotide bases, reversing the effects of methylation. These two proteins are currently the only known demethylases for m6A, playing crucial roles in the dynamic regulation of RNA function. The m6A methylation reader proteins are a class of RNA-binding proteins capable of specifically recognizing and binding to regions methylated by m6A. By doing so, they can modify RNA secondary structure, influencing protein-RNA interactions and affecting various RNA-mediated processes [13].

Numerous studies have shown that m6A modulators play significant roles in the progression of autoimmune disorders through their regulation of immune cell functions. For instance, recent research highlighted that ALKBH5 enhances Interferon-γ expression in $CD4^+$T cells, which, in turn, promotes the development of colitis in a murine model of adoptive transfer colitis [14]. Dysregulation of the m6A reader YTHDF2 has been linked to the activation of the NF-κB/TNFAIP3 signaling pathway in peripheral blood mononuclear cells (PBMCs), contributing to the promotion of systemic lupus erythematosus [15]. Similarly, METTL3, by activating the NF-κB signaling pathway, enhances the release of inflammatory factors by fibroblast-like synovial cells, exacerbating rheumatoid arthritis symptoms [10]. While the specific role of m6A modification in the aberrant immune response characteristic of SS remains to be fully elucidated, our previous research has established that the hyper-activation and atypical differentiation of $CD4^+$T cells significantly contribute to the pathology of SS [16–18]. Interestingly, a recent study has indicated that *METTL3*-deficient murine T cells are unable to expand and differentiate in response to IL-7 [19]. This study also reported that *METTL3* could regulate the function and stability of regulatory T cells (Tregs) [20]. These results indicated that the m6A modification may also play an immunomodulatory role in SS.

In the present study, we applied a machine learning approach to screen for key m6A modulators in SS. Machine learning, a cornerstone of modern artificial intelligence, has emerged as one of the most dynamic sectors, leveraging complex pattern recognition to revolutionize various domains, including medical research [21]. Its utility spans a comprehensive array of applications, from enhancing diagnostic accuracy and optimizing treatment protocols to evaluating risk factors and advancing personalized and precision

medicine [22,23]. We first utilized database gene expression profiles from databases to identify differentially expressed m6A regulators between samples taken from SS patients and healthy controls. Machine learning approaches were then used to screen key biomarkers in order to establish a diagnostic model. The obtained predictive model, based on m6A regulators, was able to accurately distinguish between SS patient and control samples. Upon stratifying SS specimens based on m6A regulator expression, our investigation delineated two distinct m6A modification landscapes. This categorization revealed profound disparities in immunocyte infiltration, immune response activation, and the spectrum of predicted biological functions across the identified patterns. These variations underscore the substantial influence of m6A modifications on the immune microenvironment in SS, reinforcing the hypothesis that m6A dynamics contribute to the pathophysiological immune dysregulation observed in SS.

2. Materials and methods

2.1. Raw data collection and preprocessing

The workflow is presented in Fig. 1. For the foundational data of our study, we downloaded human expression profiles (accession number: GSE51092) [24] from the Gene Expression Omnibus public database [25], a publicly accessible database that serves as a repository for high-throughput gene expression data. This dataset comprises the gene expression arrays of whole peripheral blood from 190 individuals diagnosed with Sjögren's syndrome and 32 healthy controls. The platform for GSE51092 was GPL6884 (Illumina HumanWG-6 v3.0 expression BeadChip). Another dataset (GSE84844) contained 60 whole blood samples, including 30 SS and 30 controls [26]. The platform for GSE84844 was GPL570 (Affymetrix Human Genome U133 Plus 2.0 Array). The clinical characteristic data for GSE84844 were also downloaded. Following the consolidation of the datasets, we undertook a meticulous annotation process for all probes, assigning them corresponding gene names to ensure the accuracy and relevance of our gene expression analysis. Probes that could not be associated with specific gene names were rigorously excluded from the datasets. In addressing the challenge of multiple probe matches per gene within our dataset, we utilized the dplyr R package, a tool renowned for its efficiency and flexibility in data manipulation. This approach allowed us to calculate the average expression levels for genes represented by multiple probes, thereby ensuring a more accurate and reliable representation of gene expression in individual samples. Subsequently, we applied quantile normalization using the limma R package to normalize the expression data [27]. To merge the data, we utilized the

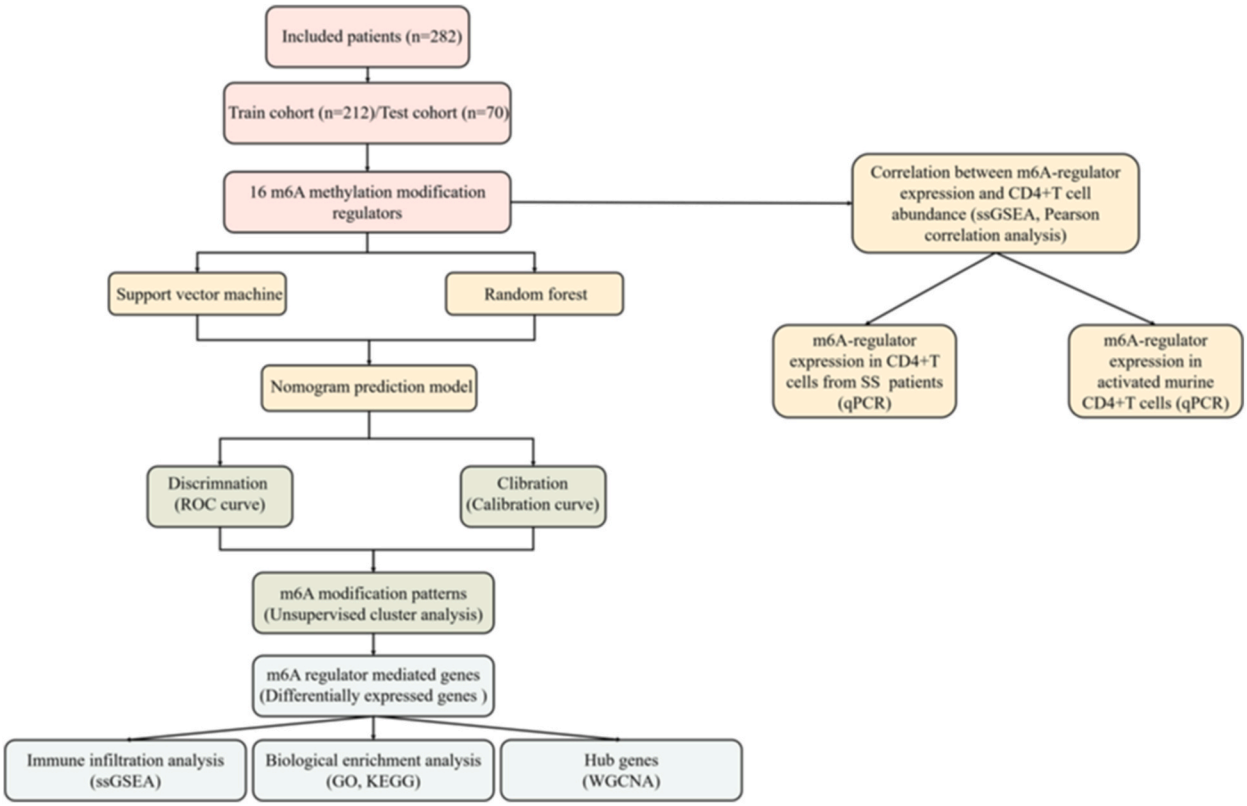

Fig. 1. Flow chart of this research programme.
GO refers to Gene Ontology; KEGG denotes the Kyoto Encyclopedia of Genes and Genomes; qPCR represents quantitative real-time PCR; the ROC curve is the receiver operating characteristic curve; ssGSEA signifies single-sample gene set enrichment analysis; WGCNA stands for weighted gene co-expression network analysis.

inSilicoMerging R package [28]. Batch differences were addressed using the Surrogate Variable Analysis (sva) R package, allowing us to account for and eliminate any confounding effects. To ensure robustness and minimize bias, we randomly divided the samples into training and validation groups, with approximately 75% and 25% of the total samples, respectively. The training set consisted of 47 control samples and 165 SS samples, while the validation set comprised 15 control samples and 55 SS samples [29]. The training set was used to establish a predictive model, which was subsequently assessed for predictive accuracy and reliability using the validation set. For comprehensive transparency and to facilitate the replication of our study's findings, detailed web links and the corresponding analytical code have been meticulously cataloged. These resources are readily accessible in Additional files 1 and 2, respectively.

2.2. Screening for SS-associated m6A regulators

The list of m6A regulators utilized in this study can be found in Additional file 3. These regulators encompass gene sets that have been reported in multiple seminal studies in the field [30–32]. We used the limma R package to identify m6A regulators that were differentially expressed between the SS and control groups according to the cut-off criteria of an adjusted p-value<0.05 and $|\log_2$ (fold change)$| > 1$ [27]. The included genes were used in subsequent analyses. Since m6A regulators often function synergistically, we used Pearson correlation analysis to test and quantify the strength of relationships.

2.3. Diagnostic model

Previous investigations have demonstrated the predictive capabilities of both random forest (RF) and support vector machine (SVM) models in identifying disease risk factors [33,34]. We screened for predictors of the best mathematical classification model for SS diagnosis using the RF model and the SVM model. The RF algorithm, renowned for its ensemble learning approach, combines multiple decision trees to form a 'forest', offering robust predictions. This method's efficacy is partly determined by the Gini coefficient, with lower values indicating greater variable importance in the model. Conversely, the SVM algorithm excels in transforming originally non-linearly separable datasets into linearly separable ones, utilizing a kernel function. The significance of variables within the SVM framework is quantitatively assessed by the discriminant function coefficient, w^2, highlighting their contribution to the model's decision-making process. For the implementation of these sophisticated algorithms, we utilized the randomForest and kernlab packages in R, capitalizing on their comprehensive functionality to conduct a thorough analysis [35,36]. In our quest to delineate the most accurate predictive model for Sjögren's Syndrome, we employed the pROC and DALEX R packages to meticulously evaluate and compare the models based on their Area Under the Receiver Operating Characteristic (ROC) Curve (AUC) values and residual analysis. This rigorous statistical assessment allowed us to discern the model that exhibits superior diagnostic precision [37,38]. Subsequent to the processes of dimensionality reduction and feature selection, we identified and harnessed the most predictive m6A regulators. These were instrumental in the construction of a nomogram within the training dataset, utilizing the rms R package. The effectiveness and diagnostic accuracy of our predictive model were further substantiated through ROC curve analysis, offering a quantifiable measure of the model's performance in distinguishing between cases of Sjögren's Syndrome and healthy controls. An AUC value of $0.7<\text{AUC}\leq 1$ indicates a gene signature with high accuracy in prediction. Furthermore, calibration plots were used to evaluate the concordance between predicted values and observed values, ensuring reliable calibration of the model.

2.4. Unsupervised cluster analysis of m6A modification patterns in SS

In our investigation into the molecular mechanisms underlying SS, we harnessed unsupervised pattern clustering to segregate SS samples based on the expression profiles of 16 m6A RNA methylation regulators. This methodological approach, facilitated by the ConsensusClusterPlus package in R, enabled the precise construction of cumulative distribution function curves for cluster numbers ranging from $k = 2$ to 9, accompanied by the calculation of delta area scores [32,39]. This rigorous analytical process informed the optimal cluster number selection, culminating in the identification of two distinct m6A modification patterns within the SS cohort. To validate the robustness of these identified subgroups, we conducted a principal component analysis (PCA), further substantiating the distinct molecular signatures of the m6A modification patterns. Our study further delved into the transcriptional disparities within Sjögren's Syndrome samples, categorizing them by distinct m6A methylation patterns. Utilizing the limma package in R, we conducted a comprehensive analysis to unearth genes whose expression levels were significantly affected by m6A regulatory mechanisms. The selection criteria for differentially expressed genes (DEGs) were stringent: only those exhibiting an absolute log fold change ($|\text{logFC}|$) greater than 1 and an adjusted p-value below 0.05 were considered significant. The identified significant DEGs were then utilized in subsequent analyses.

2.5. Relationship between m6A regulators and immune characteristics

To elucidate the immune landscape of Sjögren's Syndrome (SS) and its variation across different patient subgroups, we employed single-sample gene-set enrichment analysis (ssGSEA). This sophisticated approach, executed using the GSVA package in R, allowed for the precise estimation of the abundance of 23 types of infiltrating immune cells within the SS cohorts [40,41] (**Additional file 4**). Subsequently, we performed a comparative analysis of the enrichment scores, which serves as indicators of the relative abundance of each immunocyte, between the SS and control samples. Prior to analysis, a normality test was conducted on the data (**Additional file 5** and **6**), revealing a distribution that was relatively normal. Given the limited availability of only two datasets for each cell type (normal and SS), and considering the continuous nature of the enrichment scores, we employed a t-test for statistical comparison. To advance

our understanding of the intricate relationship between m6A regulators and the immune microenvironment in SS, we undertook a detailed correlation analysis. In this analysis, we examined the correlation (with a threshold of $|R|>0.2$ and a p-value<0.05) between gene expression and the enrichment scores of immune cells. In addition, we also assessed the activity of the immune response based on the gene sets of specific immune responses downloaded from the ImmPort database [42] (**Additional file 7**). The gene list of major histocompatibility complex (MHC)-related genes was obtained from the Human Gene Nomenclature Committee (HGNC) database [43] (**Additional file 8**). We also retrieved clinical data from GSE84844 and conducted differential analyses of the clinical characteristics among patients belonging to different m6A clusters. Notably, we observed associations between certain serological indicators, such as IgA, IgG, IgM, ANA (anti-nuclear antibodies), RF (rheumatoid factor), anti-Ro/SSA, and anti-La/SSB antibodies, and over-activated humoral immunity. Moreover, we found that a stronger activation of the humoral immune response in SS was correlated with more pronounced disease activity [26]. To assess the activity of SS, we utilized the ESSDAI (European League Against Rheumatism Sjögren's Syndrome Disease Activity Index), which encompasses 12 domains, including systemic symptoms, lymph nodes, glands, blood system, and serological changes [44]. The ESSDAI provides a comprehensive evaluation of disease activity in various aspects of SS.

2.6. Biological enrichment analysis for different m6A clusters

To elucidate the biological implications of DEGs identified, we conducted a comprehensive functional enrichment analysis. This included both Gene Ontology (GO) enrichment analysis and Kyoto Encyclopedia of Genes and Genomes (KEGG) pathway analysis, employing methodologies detailed in our previous work [45,46]. In the GO enrichment analysis, we annotated genes using the org.Hs.eg.db R package and performed enrichment analysis using clusterProfiler ($P < 0.05$) [47]. As for KEGG pathway analysis, gene annotations were obtained from the KEGG rest API and the enrichment analysis was also implemented using the clusterProfiler R package. Statistical thresholds were set at $\alpha = 0.05$.

2.7. Identification of m6A mediated genes

Following the stratification of Sjögren's syndrome (SS) samples into distinct clusters based on m6A modification patterns, we embarked on a rigorous analysis to delineate 'm6A regulator mediated genes' by identifying differentially expressed genes across the clusters. To unearth hub genes within this context, we employed Weighted gene co-expression network analysis (WGCNA), a sophisticated methodological approach designed to detect co-expressed gene modules and delineate their associations with specific phenotypes of interest. Utilizing the WGCNA package in R, our analysis was conducted on gene expression profiles from 189 SS samples, ensuring the exclusion of gene and sample outliers via the goodSamplesGenes function to maintain data integrity. The analytical process included Pearson's correlation analyses to ascertain the relationships between various gene modules and SS subgroups. Additionally, we quantified the relevance of each gene to m6A modification patterns (gene significance, GS) and assessed the congruence of gene expression profiles with module eigengenes (module membership, MM), setting a stringent threshold for hub gene identification at $|MM| > 0.8$ and $|GS| > 0.1$, in line with established precedents from prior research [48].

2.8. Acquisition of the study samples

This research received approval from the Ethics Committee of the Shanghai Ninth People's Hospital affiliated to Shanghai Jiao Tong University School of Medicine, under the approval IDs SH9H-2019-T159-2 and SH9H-2021-TK69-1. In adherence to ethical standards, all participants provided written informed consent prior to inclusion in the study. Our selection criteria for Sjögren's syndrome patients aligned with the guidelines established by the American-European Consensus Group, ensuring a focused and representative study cohort [49]. Importantly, to minimize confounding variables, none of the participants had undergone treatment with immunosuppressive or immunomodulatory drugs prior to sample collection. The study exclusively involved middle-aged female donors, aged between 30 and 60 years, from whom 10 mL of peripheral blood were collected. Peripheral blood mononuclear cells (PBMCs) were subsequently isolated following established protocols [16]. Further precision in our cellular analysis was achieved through the isolation of two subsets of human T cells from PBMCs using positive selection microbeads, specifically targeting CD4+T cells and $CD8^+$T cells (Miltenyi Biotec), in accordance with the manufacturer's guidelines. Additionally, labial gland biopsies were procured for histological examination via hematoxylin and eosin (H&E) staining, contributing to our comprehensive assessment of the pathological features of SS.

2.9. Cell culture

Female C57BL/6 mice were purchased from the Model Animal Research Center of Nanjing University. All animal procedures conformed to the principles outlined in the Guide for the Care and Use of Medical Laboratory Animals [50]. Spleens were meticulously processed over a cell strainer (Falcon) and washed in PBS supplemented with 2% fetal bovine serum (FBS, Gibco) to achieve a homogeneous single-cell suspension. Total $CD4^+$ T cells were then isolated from the splenic cell suspension using the Mouse $CD4^+$ T Cell Isolation Kit (Stemcell Technologies), as per the manufacturer's instructions. The isolated cells were cultured in a medium enriched with 10% FBS and 1% penicillin/streptomycin (HyClone), and stimulated with plate-bound anti-CD3ε and anti-CD28 antibodies (5 μg/ml, BD Biosciences) for 48 h, to facilitate further experimental analyses.

2.10. Gene expression analysis

Total RNA was meticulously extracted from isolated T cells utilizing TRIzol Reagent (TaKaRa), strictly following the manufacturer's guidelines. Subsequently, 1000 ng of the extracted total RNA was reverse-transcribed into complementary DNA (cDNA) employing the PrimeScript RT reagent kits (TaKaRa). This cDNA served as the template for subsequent quantitative real-time PCR (qPCR) analyses, which were conducted on a LightCycler 96 Instrument (Roche) to assess the expression levels of specific genes of interest. Primer sequences utilized for qPCR are detailed in Table 1, with ACTB/Actb acting as the internal mRNA control to normalize the data. To ensure the robustness and reproducibility of our findings, all qPCR experiments were performed in triplicate. The relative expression levels of RNA were quantitatively determined using the 2-△△Ct method.

2.11. Statistical analysis

Statistical computations and analyses were executed using R software version 4.1.1, supplemented by Bioconductor packages, as outlined in **Additional File 1**. Adhering to stringent statistical practices, all tests conducted were two-tailed, employing a significance threshold (α) of 0.05. Differences of statistical significance were annotated accordingly: * indicating $p < 0.05$; ** for $p < 0.01$; *** denoting $p < 0.001$; and **** representing $p < 0.0001$.

3. Results

3.1. Genetic variation of m6A regulators and immune activation SS

After applying batch effect elimination techniques, we observed that the distribution of data became consistent among the datasets (Fig. 2A and B, Additional file 9). This consistency in data distribution indicates that the batch effects, which could introduce variations and bias in the data, were successfully removed. Based on stratified random sampling, the dataset was divided into training and validation cohorts. The training set contained 165 SS and 47 controls, while the validation set contained 55 SS and 15 controls (**Additional file 10**). In our endeavor to delineate the role of m6A modifications within the immune microenvironment, we embarked on a comprehensive sorting and classification of 28 m6A regulators, employing a schematic diagram to depict the dynamic interplay of these modifiers (Fig. 2C, **Additional file 3**). Initial analysis focused on the expression profiles of m6A regulators within our training cohort, identifying 16 pivotal regulators (Fig. 2D). Among these, *YTHDC1* and *ALKBH5* exhibited basal expression levels surpassing those of their counterparts, indicating their potential prominence in m6A regulatory processes. Subsequent differential expression analysis revealed notable disparities among 7 regulators—*YTHDF3*, *RBM15*, *YTHDC2*, *YTHDF1*, *RBM15B*, *ELAVL1*, and *ALKBH5*—across the examined cohorts. Notably, *YTHDC2* emerged with the highest fold change, closely followed by *YTHDF3*, underscoring their significant modulation in the context of SS. In contrast, the expression of *RBM15B*, *YTHDF1*, *ELAVL1*, and *ALKBH5* was markedly reduced in SS patients, illustrating a pattern of regulatory downregulation. These findings were succinctly captured in a heatmap plot (Fig. 2E), illustrating the expression landscapes of the differentially expressed m6A regulators. Further correlation analysis enhanced our understanding of the regulatory network, highlighting a positive association between *METTL3* and a subset of

Table 1
A list of Primers.

Gene and primer type	Primer sequences (5′ to 3′)
Actb	
Forward primer	GATCAAGATCATTGCTCCTCCTG
Reverse primer	AGGGTGTAAAACGCAGCTCA
ACTB	
Forward primer	AACGACCCCTTCATTGAC
Reverse primer	TCCACGACATACTCAGCAC
Mettl3	
Forward primer	CTGGGCACTTGGATTTAAGGAA
Reverse primer	TGAGAGGTGGTGTAGCAACTT
METTL3	
Forward primer	GAGATATGCTCTTAACCACCCG
Reverse primer	GCTGCCCAATCCATCCAA
Ythdf1	
Forward primer	ACAGTTACCCCTCGATGAGTG
Reverse primer	GGTAGTGAGATACGGGATGGGA
YTHDF1	
Forward primer	ACCTGTCCAGCTATTACCCG
Reverse primer	TGGTGAGGTATGGAATCGGAG
Alkbh5	
Forward primer	CGCGGTCATCAACGACTACC
Reverse primer	ATGGGCTTGAACTGGAACTTG
ALKBH5	
Forward primer	CCAGCTATGCTTCAGATCGCCT
Reverse primer	GGTTCTCTTCCTTGTCCATCTCC

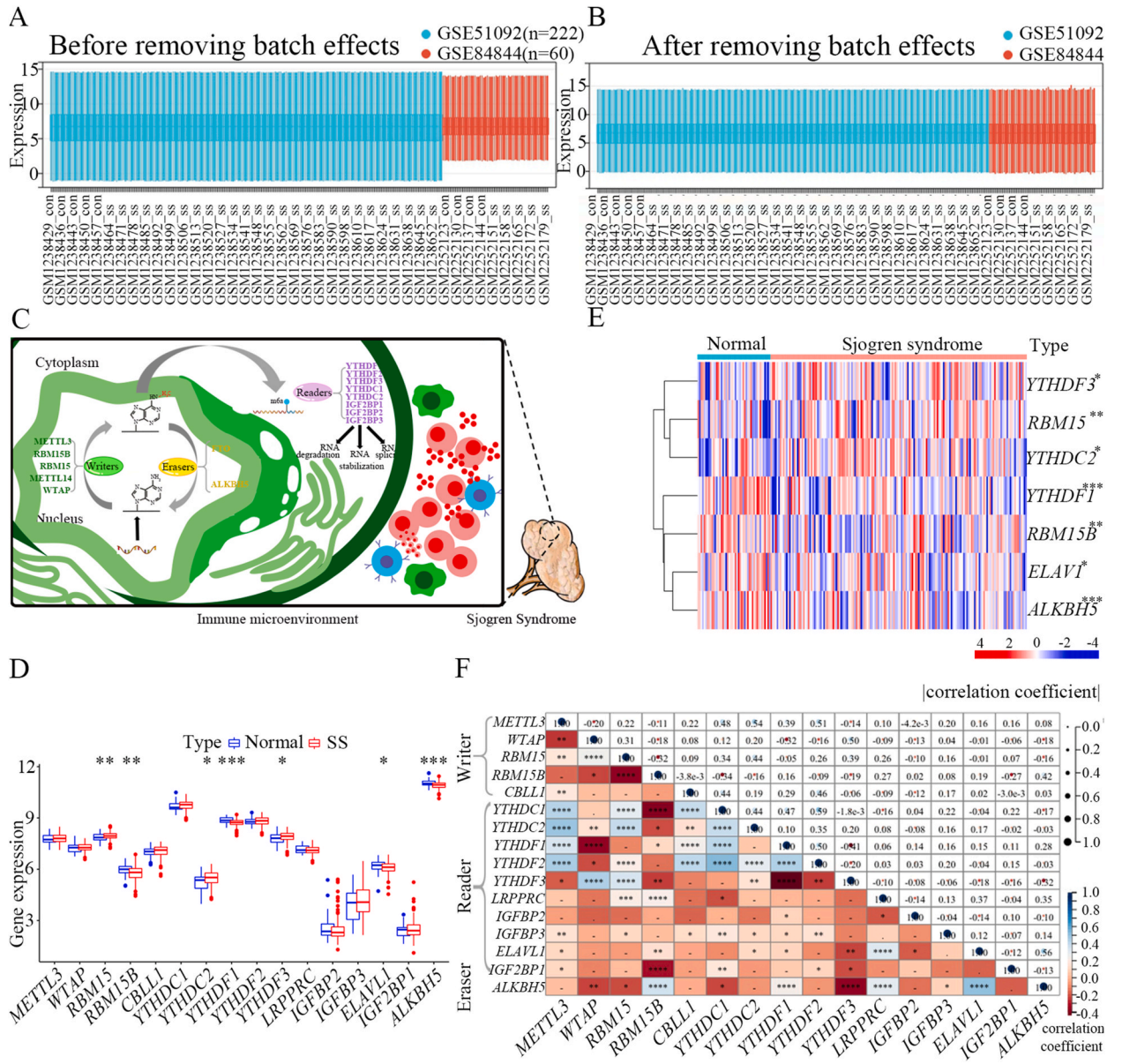

Fig. 2. Identification of differentially expressed m6A regulators

(A–B) The distribution of mRNA expression levels for two datasets before removing batch effects (A) or after removing batch effects (B).

(C) Overview of m6A RNA methylation in Sjögren's syndrome, showing the roles of 'writers' (methylation addition), 'erasers' (methylation removal), and 'readers' (methylation interpretation) and their impact on RNA functionality, contributing to the disease's pathogenesis.

(D) Violin plot illustrating the expression differences of 16 m6A-related genes between Sjögren's syndrome patients and healthy controls. Significance levels are marked as follows: $*p < 0.05$, $**p < 0.01$, $***p < 0.001$ versus control group.

(E) Heatmap displaying expression variations of seven differentially expressed m6A methylation regulators between Sjögren's syndrome and normal individuals. Significance levels are denoted as: $*p < 0.05$, $**p < 0.01$, $***p < 0.001$ compared to the control group.

(F) Correlation analysis based on the expression of 16 m6A regulators.

m6A regulators, including *YTHDC1*, *YTHDC2*, *YTHDF1*, and *YTHDF2* (Fig. 2F). This suggests *METTL3*'s role in the recruitment and interaction with these proteins, a pivotal aspect of the m6A modification process [51,52]. Among these relationships, the correlation between *YTHDC1* and *YTHDF2* was particularly notable, boasting the highest coefficient (r = 0.59), hinting at intricate regulatory dynamics within the m6A landscape.

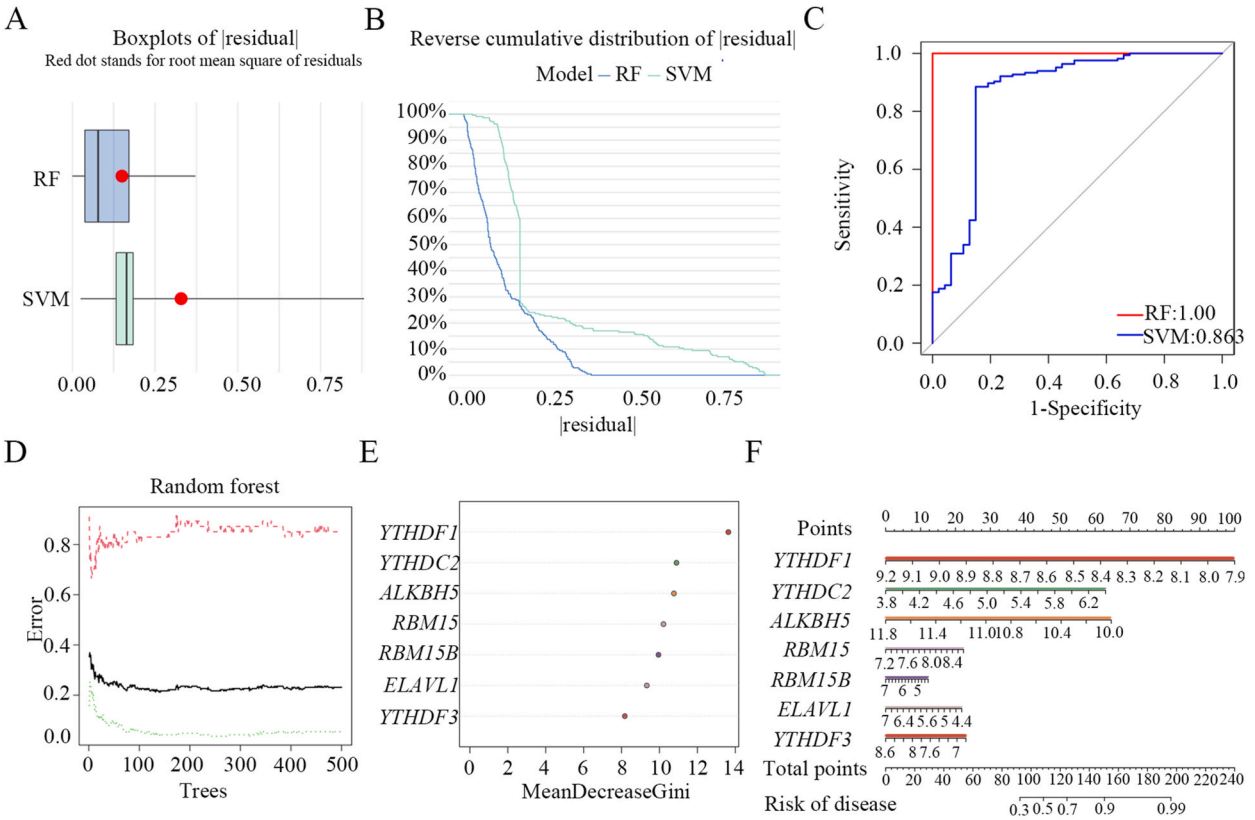

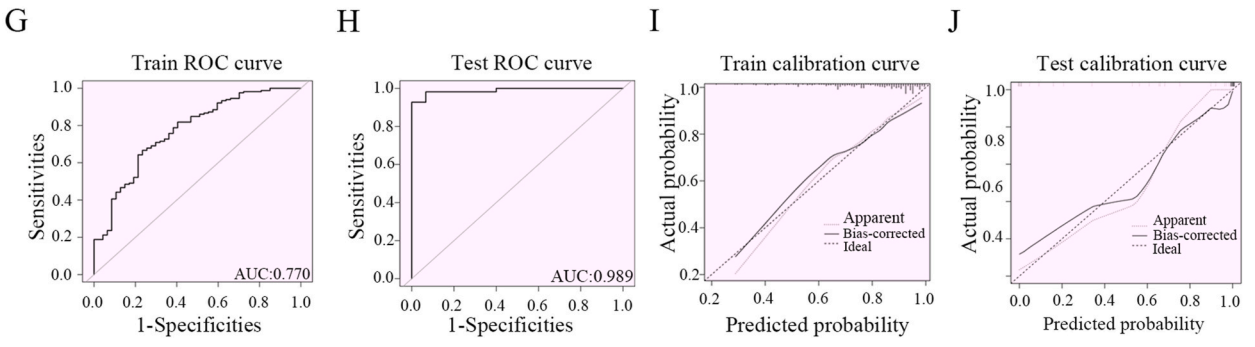

(caption on next page)

Fig. 3. Construction and validation of a nomogram model for SS diagnosis
(A) Residual boxplot comparing the performance of Random Forest (RF) and Support Vector Machine (SVM) algorithms, illustrating the distribution of residuals for each method to assess model accuracy and predictive reliability.
(B) Cumulative residual distribution map of the samples analyzed using Random Forest (RF) and Support Vector Machine (SVM) algorithms. The plot highlights the relationship between the number of outliers and the magnitude of residuals, with the vertical position of the line indicating the cumulative size of residuals across the sample population, reflecting model precision and outlier impact.
(C) ROC curves for Random Forest (RF) and Support Vector Machine (SVM) models, demonstrating their prediction accuracy through the area under the curve (AUC). A larger AUC indicates greater model precision in distinguishing between classes.
(D) Visualization of the relationship between the number of classification trees in a Random Forest (RF) model and the classification error. The graph illustrates how increasing the number of trees contributes to a gradual reduction in classification error, indicating the model's stabilization and improved reliability in biomarker screening.
(E) Chart depicting the Gini index of predictors in the Random Forest (RF) model, illustrating the relative importance of each predictor. A higher Gini index indicates a greater influence of the predictor on the model's decision-making process.
(F) Nomogram for predicting the risk of Sjögren's syndrome utilizing the expression levels of seven m6A regulators.
(G–H) Graphs depicting the predictive accuracy of the m6A regulator gene signature in both the derivation (G) and validation (H) cohorts, as measured by the pooled area under the curve (AUC). An AUC value greater than 0.7 and up to 1 signifies high predictive accuracy of the gene signature for assessing the risk of Sjögren's syndrome (SS). The ROC curve shows that the nomogram model constructed from the seven m6A regulators has optimal predictive power. The AUCs were 0.770, and 0.989 in the training and test cohorts, respectively.
(I–J) Calibration curve evaluating the predictive accuracy of the nomogram model for Sjögren's syndrome (SS) risk assessment.

3.2. Construction and validation of an m6A-based diagnostic model

To further restrict the range of m6A regulators, the RF and SVM algorithms were used to construct two different models based on the 7 differentially expressed m6A regulators. As shown in Fig. 3A, the median residuals obtained by the RF algorithm were lower, implying greater accuracy in the RF model. The reverse cumulative distribution plot also showed that the residuals of most samples of the RF model were relatively lower (Fig. 3B). In the comparative analysis of machine learning models for Sjögren's Syndrome (SS) classification, the Random Forest (RF) model demonstrated superior performance over the Support Vector Machine (SVM), as evidenced by higher Area Under the Receiver Operating Characteristic (ROC) Curve (AUC) values (Fig. 3C). This finding is graphically represented in Fig. 3D, which details the inverse relationship between RF iteration times and classification error, revealing a convergence to minimal error rates at 300 iterations. This optimization underscores the RF model's robustness in SS sample classification. Further analysis within the RF framework prioritized seven m6A regulators—*YTHDF3*, *RBM15*, *YTHDC2*, *YTHDF1*, *RBM15B*, *ELAVL1*, and *ALKBH5*—based on their significant Gini index values (Fig. 3E), all exceeding a threshold of 2, highlighting their predictive utility [53]. Utilizing these seven critical regulators, we constructed a predictive nomogram model (Fig. 3F). Its discriminative and calibration capabilities were rigorously assessed via ROC and calibration curve analyses, respectively. The nomogram yielded an AUC of 0.770 for the derivation set and an impressive 0.989 for the validation set, indicating excellent discriminative power between control and SS samples (Fig. 3G and H). Moreover, the calibration curve illustrated minimal deviation between observed and predicted outcomes, attesting to the nomogram's high predictive accuracy (Fig. 3I and J). These compelling results illuminate the pivotal role of the identified m6A regulators in SS progression, suggesting their potential as biomarkers and therapeutic targets.

3.3. Relationship between m6A regulators and the immune microenvironment

Our investigation into the immune microenvironment of Sjögren's Syndrome (SS) patients reveals distinctive patterns of immune cell infiltration, as depicted in Fig. 4A. Specifically, we observed a pronounced increase in activated B cells, $CD4^+$ T cells, and Th17 cells within SS patients compared to controls, aligning with prior evidence that highlights hyperactivation of $CD4^+$ T [17,18,54] and B cells [55,56] as hallmark features of SS pathogenesis. Intriguingly, these insights were derived from peripheral blood samples, offering a non-invasive alternative to traditional salivary gland biopsies. This is particularly relevant given reports of altered $CD4^+$:$CD8^+$ and Th17:Treg ratios in SS's early stages, underscoring systemic immune dysregulation [57]. Further extending our analysis to transcriptional data from labial gland tissues [58] confirms the heightened presence of activated $CD4^+$T and B cells in SS-affected glands (Fig. 4B), corroborated by histopathological examination which revealed significant lymphocytic infiltration and acinar disruption in SS patients (Fig. 4C and D). These findings across blood and glandular tissues underscore the pervasive nature of immune activation in SS.

Parallel to these observations, we explored the role of m6A methylation in modulating the SS immune landscape. Fig. 4E illustrates a positive correlation between the abundance of activated $CD4^+$T cells and the expression of several m6A regulators, including *METTL3*, *WTAP*, *RBM15*, *YTHDC2*, *YTHDF3*, *LRPPRC*, *IGFBP3*, and *ALKBH5*. A similar correlation pattern was observed for activated $CD8^+$T cells, underscoring the broad influence of m6A modifications on T cell dynamics. Interestingly, regulatory T cells (Tregs), critical for immune homeostasis, showed a complex correlation with m6A regulators, suggesting a nuanced role of m6A in immune regulation. Notably, our analysis did not reveal a significant correlation between activated B cells and m6A-regulated genes, indicating a selective impact of m6A modifications across different immune cell types.

3.4. The expression of m6A-regulators in activated $CD4^+$ T cells

To substantiate our correlation analysis findings regarding m6A modification's role in the immune microenvironment of Sjögren's

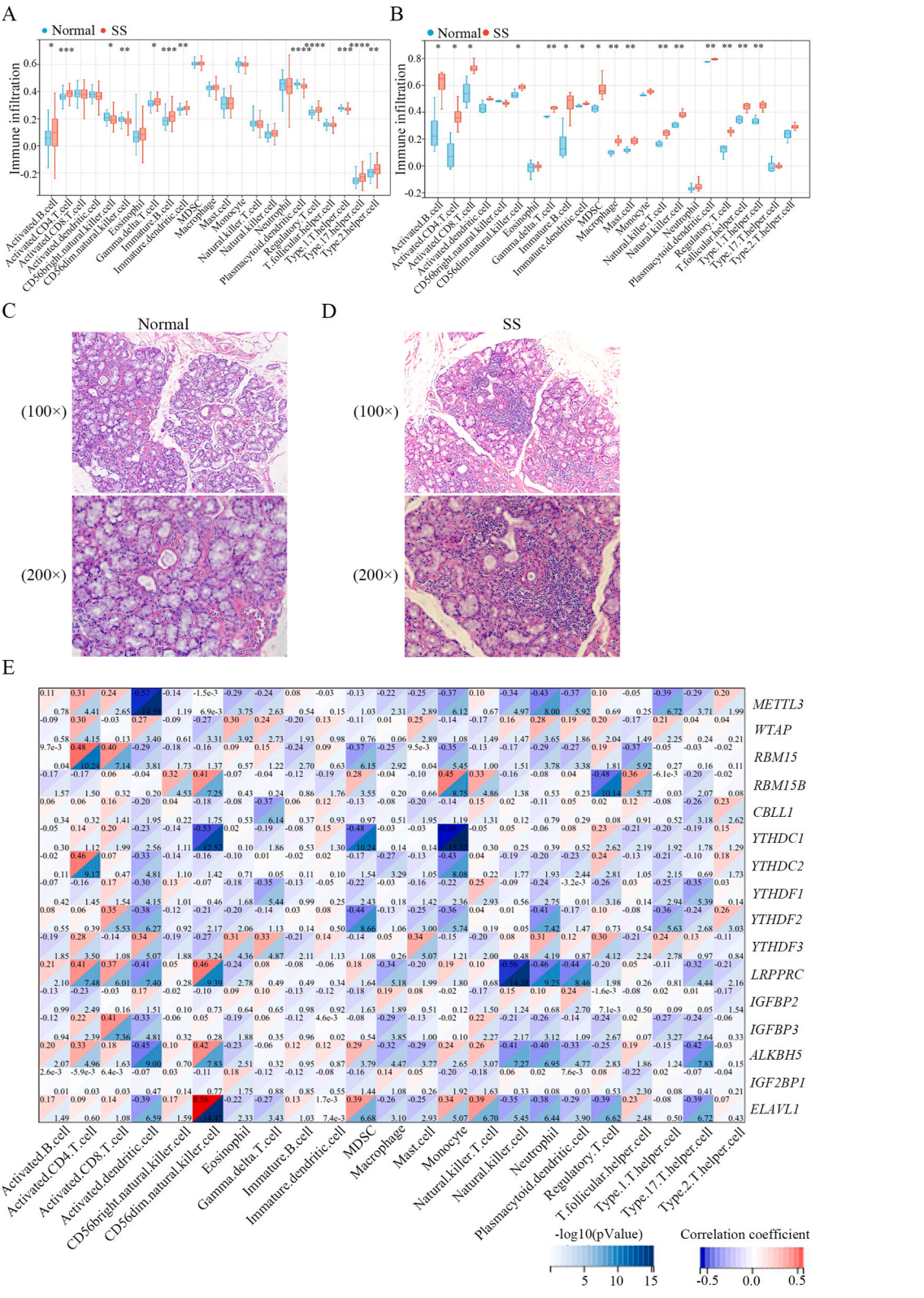

(caption on next page)

Fig. 4. The correlation between m6A regulators and immune microenvironment characteristics
(A) Comparison of immunocyte infiltration levels in peripheral blood samples between Sjögren's syndrome patients and healthy donors.
(B) Analysis of immunocyte infiltration in labial gland samples from Sjögren's syndrome patients compared to healthy donors.
(C–D) Hematoxylin and eosin (H&E) staining of labial gland samples from normal donors (C) and Sjögren's syndrome patients (D).
(E) Correlation matrix illustrating the association between m6A regulators (*METTL3*, *WTAP*, *RBM15*, *YTHDC2*, *YTHDF3*, *LRPPRC*, *IGFBP3*, *ALKBH5*) and the infiltration levels of 23 immune cell types. Specifically, it highlights a positive correlation between the abundance of activated $CD4^+$ T cells and the listed m6A regulators, suggesting their influence on immune cell dynamics. $|R|>0.2$ and $p < 0.05$ were considered significant.

Syndrome (SS), we conducted a comparative gene expression analysis of $CD4^+$ and $CD8^+$ T cells derived from SS patients and healthy donors. This analysis revealed a marked up-regulation of *METTL3*, *ALKBH5* and *YTHDF1* mRNA levels in T cells from SS patients, as illustrated in Fig. 5A and **B**. Further leveraging previously acquired sequencing data [59], we depicted the expression profiles of

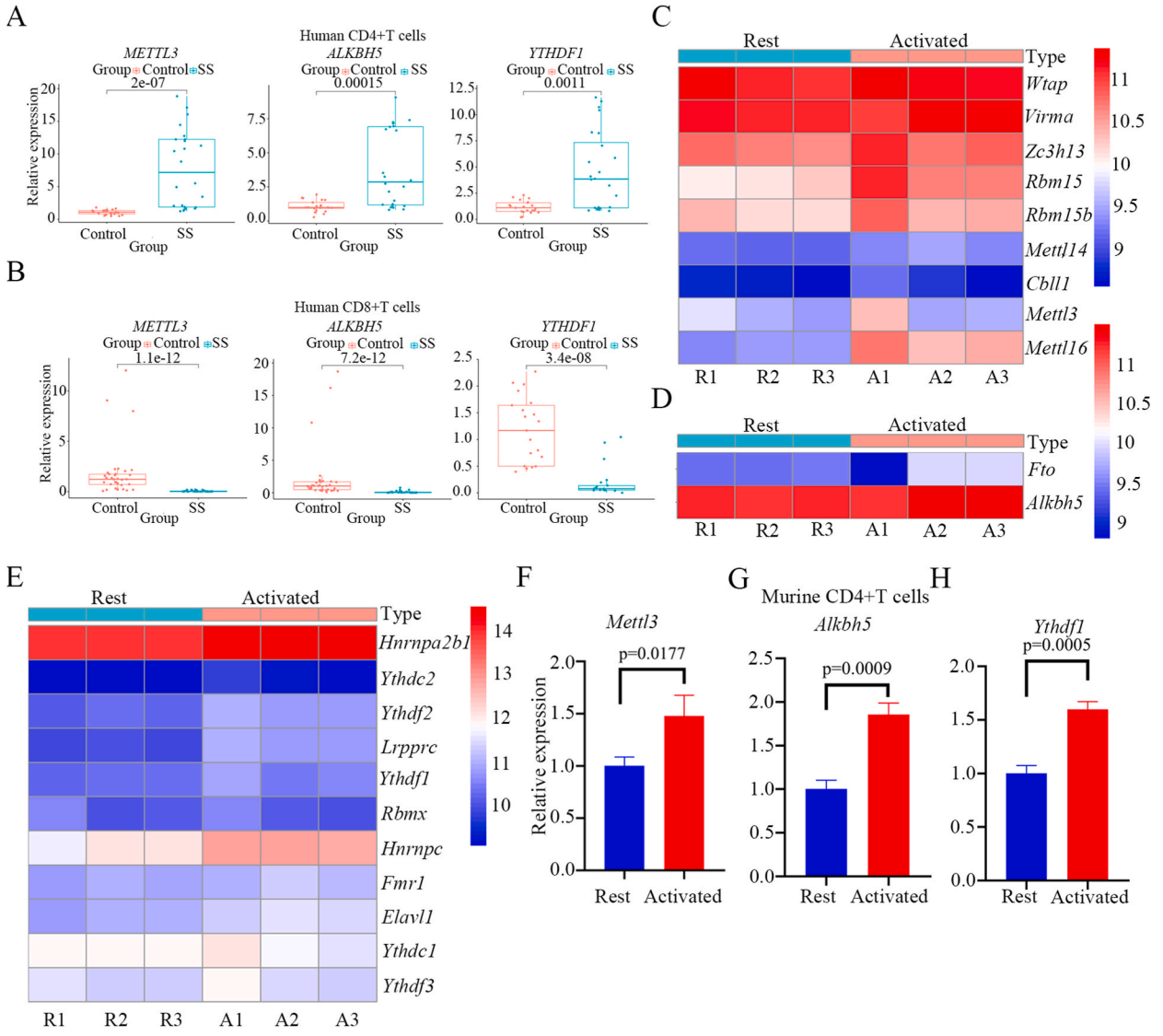

Fig. 5. M6A regulators are related to $CD4^+$T cell activation and the occurrence of SS
(A) Comparative analysis of total $CD4^+$T cells isolated from 9 healthy donors and 7 Sjögren's syndrome (SS) patients. Gene expression levels were normalized to *β-ACTIN* expression.
(B) Analysis of total $CD8^+$T cells isolated from 9 healthy donors and 7 SS patients, with gene expression normalized to *β-actin* expression.
(C–E) Heatmap displaying the expression of m6A regulators in murine $CD4^+$ T cells, comparing resting states to activated conditions.
(F–H) Murine $CD4^+$T cells were cultured in the presence of 5 μg/ml plate-bound anti-CD3ε and 2 μg/ml anti-CD28 for indicated time points. The expression of m6A regulators were evaluated by real-time PCR. Gene expression was normalized to *β-actin* expression. Data shown are means ± SD. Three independent experiments were performed for qPCR assays.

m6A-regulated genes in resting and activated CD4$^+$ T cells through comprehensive heatmap analyses (Fig. 5C–E). *Wtap*, *Virma*, *Zc3h13*, *Rbm15*, *Rbm15b*, *Hnrnpa2b1*, and *Alkbh5* were expressed at higher levels in splenic CD4$^+$ T cells. To validate these observations in vitro, we examined the expression of *Mettl3*, *Alkbh5*, and *Ythdf1* in activated CD4$^+$ T cells. The results confirmed significant upregulation of these genes in the activated CD4$^+$ T cells, which was consistent with the predicted results (Fig. 5F–H).

3.5. Expression patterns based on 16 m6A methylation modification regulators

In our quest to unravel the epigenetic landscape of SS, we categorized our dataset based on the expression profiles of 16 pivotal m6A modulators, leading to the identification of distinct m6A modification patterns within SS patients (Fig. 6A–C). Given that k = 2 was the best choice , we obtained two distinct patterns, where subgroup A contained 109 samples and subgroup B had 56 samples. Principal Component Analysis (PCA) vividly illustrated the demarcation between these clusters (Fig. 6D), further substantiated by a heatmap of the 16 m6A regulators' expression levels, delineating the variances across clusters (Fig. 6E). A subsequent differential analysis revealed alterations in 11 m6A regulators between the subgroups (Fig. 6F), with *WTAP*, *RBM15*, *YTHDF3*, *YTHDC2*, and *IGF2BP1* exhibiting higher expression in Pattern A. Conversely, Pattern B was characterized by elevated expression of *RBM15B*, *CBLL1*, *YTHDF1*, *YTHDF2*, *IGFBP2*, and *IGFBP3*. There is cross interaction or competition between the different m6A reader proteins which constitute an interactive network. The highly expressed reader proteins in different groups may exert their intracellular functions, including in mRNA decay, mRNA stabilization, and enhanced translation. These results suggest that SS is associated with distinct m6A modification patterns.

Delving into the correlation between m6A modification patterns and the immune microenvironment, we identified distinct

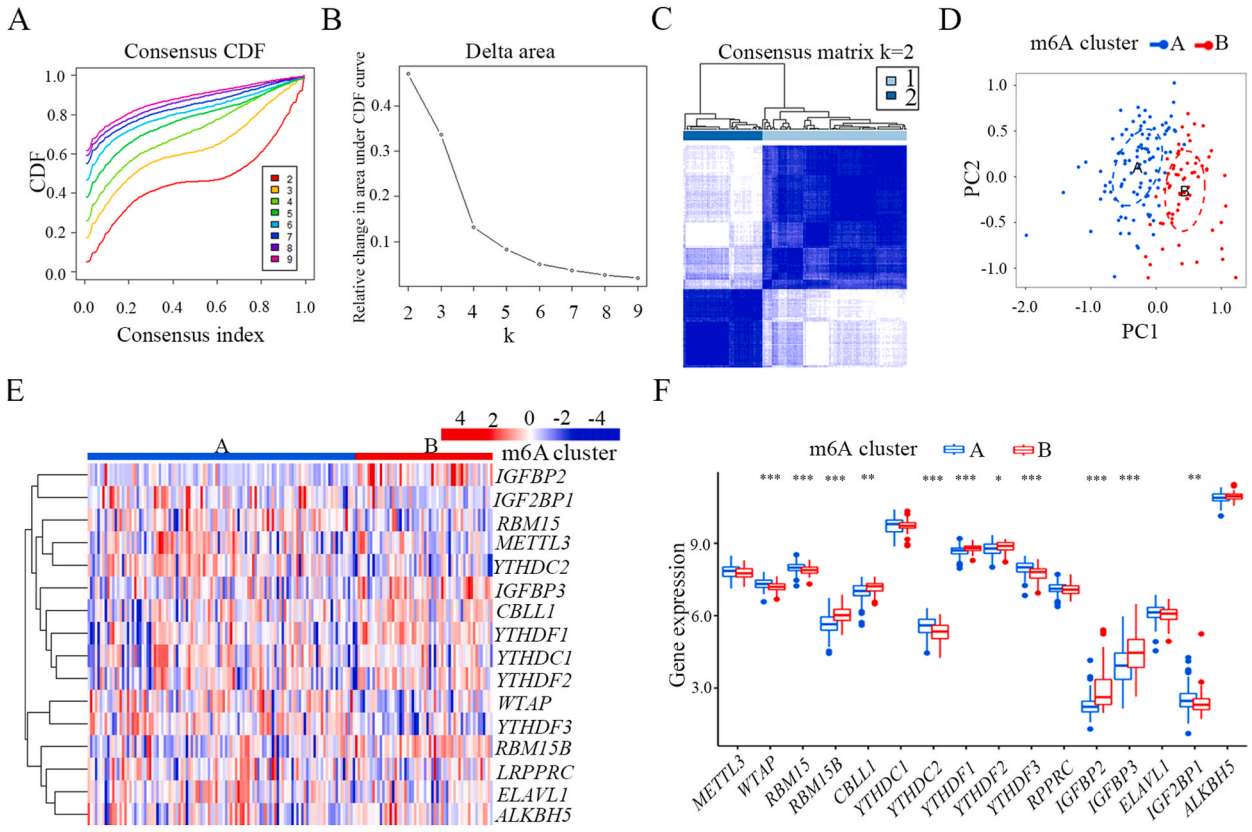

Fig. 6. Two distinct m6A modification pattern subtypes in SS

(A) Cumulative distribution function (CDF) curves for consensus matrices across cluster numbers k = 2 to 9, illustrating the stability and cohesiveness of clusters formed at different k values to determine the optimal clustering solution for the data analysis.

(B) Graph showcasing the relative changes in the area under the Cumulative Distribution Function (CDF) curve for varying cluster numbers (k = 2 to 9).

(C) Consensus clustering of the 165 SS samples for k = 2.

(D) Principal Component Analysis (PCA) of transcriptome profiles across two m6A modification subtypes, demonstrating significant transcriptomic divergence between distinct m6A modification patterns, underscoring the profound impact of m6A methylation on gene expression landscapes.

(E) Heatmap of 16 m6A regulators in different m6A modification patterns.

(F) Comparative analysis of the expression levels of 16 m6A regulators between two m6A subtypes. Significance levels are denoted with asterisks: *p < 0.05, **p < 0.01, ***p < 0.001 compared to the control group, illustrating differential expression across m6A modification patterns.

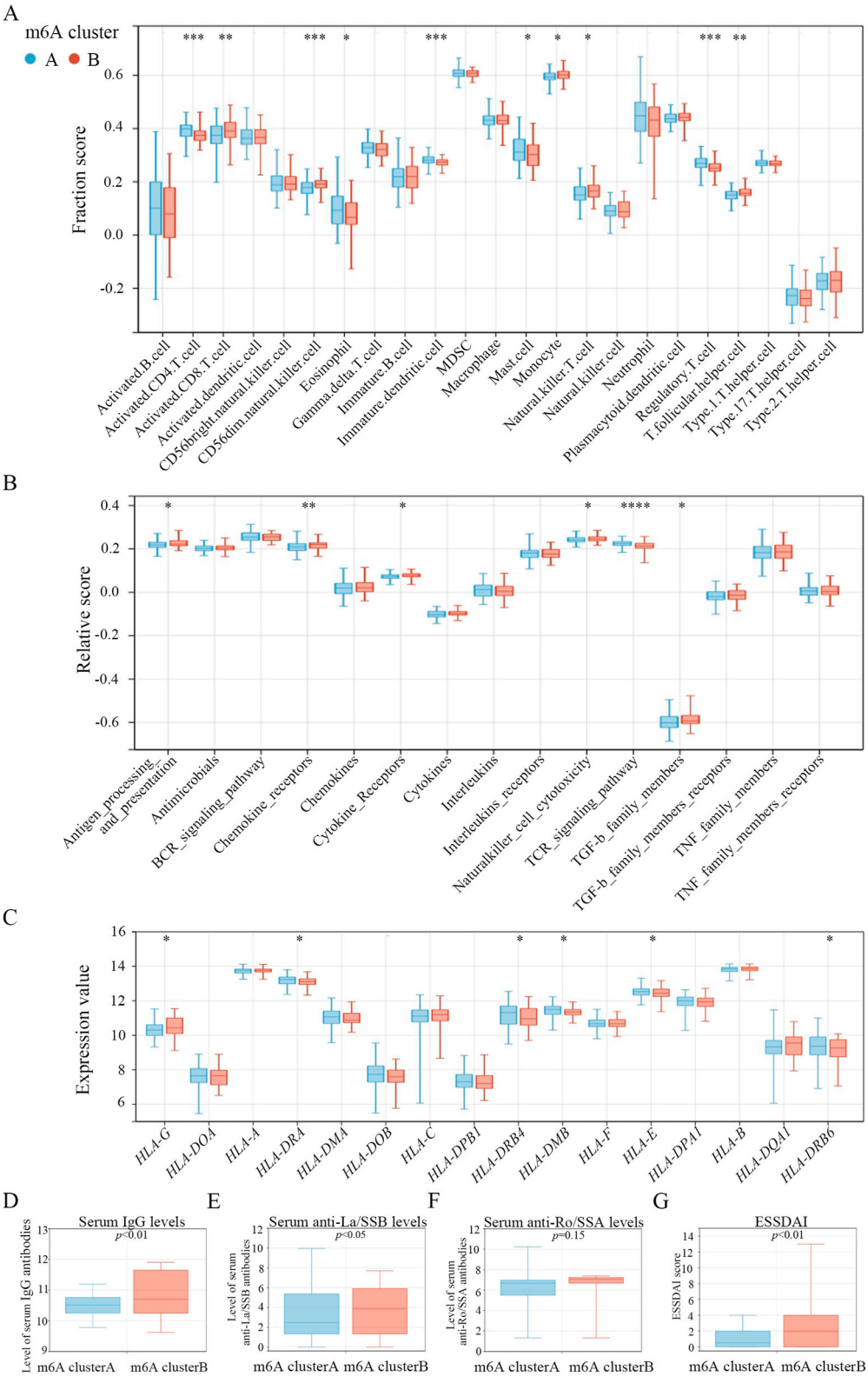

(caption on next page)

Fig. 7. Diversity of immune microenvironment characteristics between two distinct m6A modification patterns
(A) Bar graph depicting the abundance differences of infiltrating immunocytes within the immune microenvironment across two m6A modification patterns. Significance levels are marked: $*p < 0.05$, $**p < 0.01$, $***p < 0.001$ compared to the control.
(B) Bar chart illustrating the activity differences of immune reaction gene sets between two m6A modification patterns. Significance is indicated as follows: $*p < 0.05$, $**p < 0.01$, $****p < 0.0001$ compared to control, showcasing the divergent immune responses associated with each pattern.
(C) Comparison of expression levels for each MHC-related gene between two m6A modification patterns. An asterisk denotes significance at $p < 0.05$ compared to control.
(D–F) Serum levels of IgG (D), anti-La/SSB (E) and anti-Ro/SSA (F) antibodies across different m6A clusters in patients with Sjögren's syndrome. SSA refers to Sjögren's syndrome type A antigen; SSB refers to Sjögren's syndrome type B antigen.
(G) Distribution of ESSDAI (European League Against Rheumatism Sjögren's syndrome Disease Activity Index) scores among patients across different m6A modification clusters.

immunocyte compositions corresponding to each pattern (Fig. 7A). Pattern A was associated with a higher infiltration of activated $CD4^+$T cells, immature dendritic cells, and Tregs, while Pattern B favored activated $CD8^+$T cells, monocytes, and T follicular helper cells. This distinction suggests that unique m6A modification patterns may preferentially influence different immune cell types. Notably, Pattern B displayed heightened immunoreactivity, as evidenced by the upregulation of pathways critical for immune response, including antigen processing, chemokine and cytokine receptors, TCR signaling and TGF-beta family members (Fig. 7B). In m6A cluster A, activation of the TCR signaling pathway was up-regulated, suggesting that $CD4^+$ T cell activation may be up-regulated, which is consistent with the results of the cell infiltration analysis. The TGF-β signaling pathway, which acts as a suppressor of autoimmune T cell activation, had a low enrichment fraction in both clusters, also potentilly contributing to the autoimmune responses. We also analyzed MHC-related genes for differential expression in two m6A modification patterns (Fig. 7C). Compared with m6A modification pattern B, the expression levels of four MHC class II molecules (*HLA-DRA*, *HLA-DRB4*, *HLA-DMB*, and *HLA-DRB6*) and one MHC class I molecule (*HLA-E)* were higher in m6A modification pattern A. The enhanced expression of MHC class II molecules is a key component of many autoimmune mouse models, including experimental allergic encephalomyelitis, and is one of the necessary conditions for the increase of autoimmune $CD4^+$ T cells [60]. This suggests that Pattern A may represent an earlier stage of SS, characterized by elevated $CD4^+$ T cell counts and TCR signaling pathway activation. In turn, patients with m6A modification pattern B are likely to be in the middle or late stages of SS, during which $CD4^+$ T cells and B cells in peripheral blood are somewhat depleted. Subsequently, our results showed that the serum IgG and anti-La/SSB levels of m6A cluster B patients were significantly higher than those in cluster A (Fig. 7D–F). According to the ESSDAI classification, most of our samples were from patients with mild symptoms; the ESSDAI scores of patients in the two m6A clusters were statistically different. The mean scores of cluster B were greater than those of group A, suggesting that patients in group B may be in a more advanced stage of SS (Fig. 7G). Taken together, we speculate that compared with pattern B, the immunophenotype of m6A modification pattern A is more similar to the early stage of SS, which is more in line with our research field [16–18].

3.6. Biological characteristics of distinct m6A modification patterns

In our pursuit to elucidate the impact of m6A modification patterns on the pathogenesis of Sjögren's Syndrome, we embarked on a comprehensive functional enrichment analysis. This analysis utilized differentially expressed genes (DEGs) between two distinct m6A modification subgroups, uncovering a total of 1172 DEGs. Gene Ontology (GO) enrichment analysis illuminated that these DEGs predominantly contribute to protein modification processes, cytokine responses, and immune system regulation, offering substantial evidence of m6A methylation's involvement in SS's immune dynamics (Fig. 8A, **Additional file 11**). The MAPK signaling pathway emerged as notably enriched among the DEGs, underscoring its pivotal role in SS pathology (Fig. 8B, Additional file 12). Given its established connections to B cell migration, symptom alleviation in experimental SS models [61], and the regulation of autophagy and apoptosis in salivary glands [62], our findings further validate the MAPK pathway's critical function in SS. Additionally, lncRNA *NEAT1*'s promotion of MAPK activation in T cells aligns with our observations, reinforcing the pathway's significance in SS progression [17]. Subsequently, we performed WGCNA analysis based on the above DEGs (Fig. 8C). Fig. 8D and **E** indicate that the minimum soft threshold for building a scale-free co-expression network is 14. According to the optimal soft threshold, we constructed a co-expression network and divided genes into four different network modules as shown in Fig. 8F. Among these modules, the grey invalid module is a gene set consisting of genes that do not belong to any other module. After a correlation analysis between modules and m6A modification patterns, we found that the turquoise-colored module was positively correlated with m6A modification pattern A and had the highest correlation coefficient (Fig. 8G). Since the immune signature in m6A modification pattern A is closer to that of the early SS lesions that we are most interested in, we chose this module as the key module. A positive correlation between module membership (MM) and gene significance (GS) within the turquoise module (Fig. 8H) highlighted genes central to both the module and m6A modification patterns. To delineate the interactive landscape of these pivotal genes, we employed Cytoscape, crafting a protein-protein interaction (PPI) network that visualizes their interrelations (Fig. 8I) [63]. Furthermore, we executed a strategic intersection of significant genes within the turquoise module—characterized by a module membership (MM) greater than 0.8 and gene significance (GS) above 0.1—with key genes from the protein-protein interaction (PPI) network, identified by a node degree exceeding 5 (**Additional file 13**). As a result, *COMMD8* and *SRP9* were identified as hub genes.

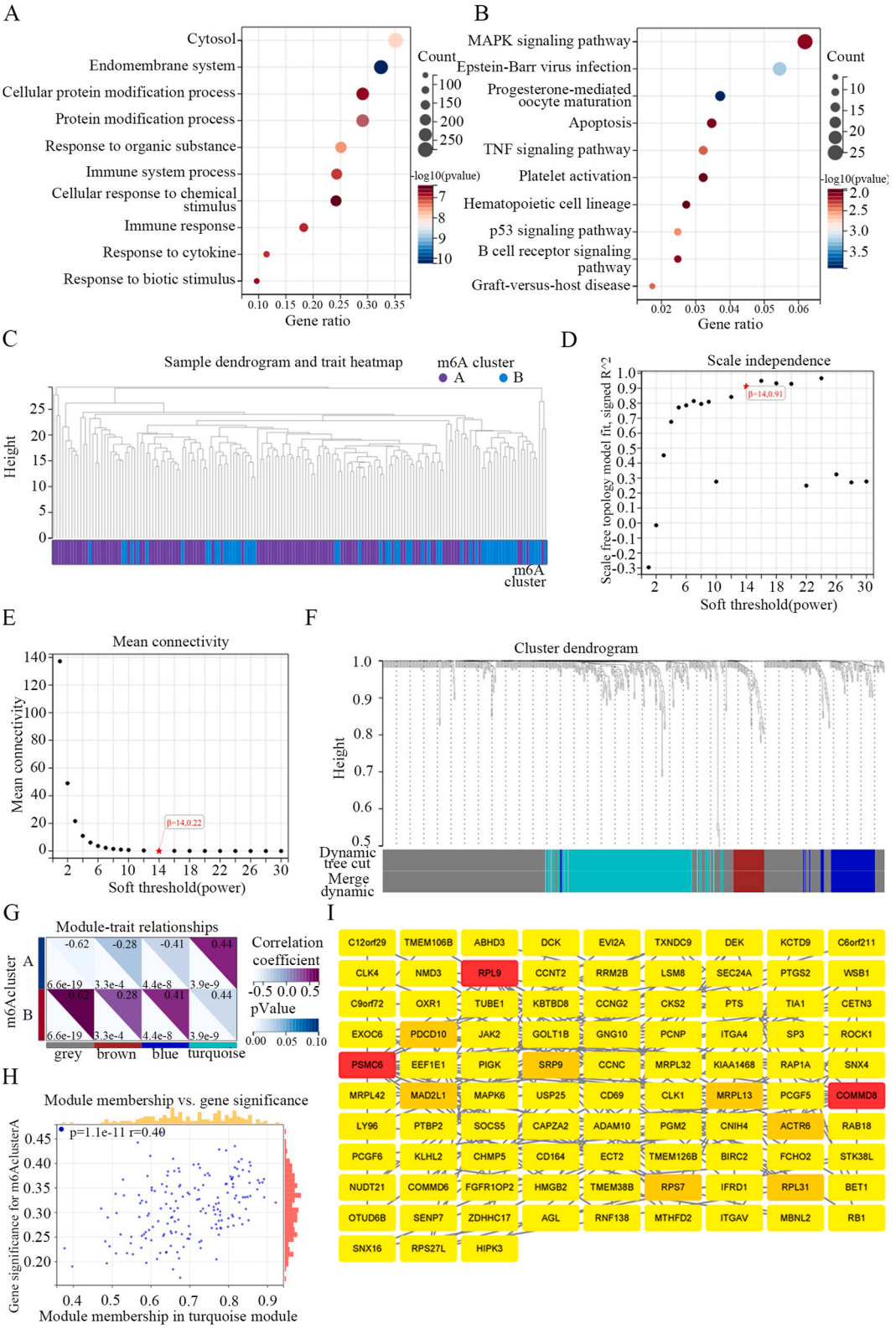

(caption on next page)

Fig. 8. Identification and function analysis of m6A phenotype-related genes in SS
(A) Bubble chart showcasing the top 10 most significant Gene ontology terms, with varying colors indicating different levels of statistical significance (*p* values).
(B) Visualization of the top 10 most significant pathway terms, categorized by varying colors to denote different levels of statistical significance (*p* values).
(C) Clustering dendrogram of two m6A modification subtypes in SS.
(D–E) Graphs depicting the analysis of the scale-free fitting index (D) and the mean connectivity (E) across a range of soft-thresholding powers from 1 to 30.
(F) Gene dendrogram resulting from average linkage hierarchical clustering, with the color row below indicating module assignments based on dynamic tree cut methodology. Four distinct modules have been identified, each represented by a unique color, showcasing the grouping of genes into modules based on their expression patterns.
(G) Heatmap displaying the correlations between module eigen genes and two distinct m6A modification patterns.
(H) Scatterplot illustrating the relationship between gene significance (GS) for m6A modification pattern A and module membership (MM) in the turquoise module. The plot reveals a highly significant correlation, suggesting that hub genes within the turquoise module are closely associated with m6A modification pattern A, highlighting their pivotal role in this specific epigenetic context.
(I) Visualization of a protein-protein interaction (PPI) network derived from genes within the turquoise module. Nodes are color-coded based on their degree of interaction: red for a node degree greater than 9, orange for a node degree greater than 5, and yellow for a degree less than or equal to 5. (For interpretation of the references to color in this figure legend, the reader is referred to the Web version of this article.)

4. Discussion

Sjögren's Syndrome (SS) represents a complex autoimmune disorder marked by the dysregulation of T cells, the aberrant production of autoantibodies, and the development of ectopic germinal centers. While there has been significant progress in delineating the pathophysiological underpinnings of SS, the clinical management of the disease is often complicated by its intrinsic heterogeneity. In this context, the exploration of epigenetic mechanisms, particularly m6A RNA methylation modifications, emerges as a promising frontier in autoimmunity research. Patients with autoimmune disorders such as rheumatoid arthritis show higher PBMC RNA N6-methyladenine that is accompanied by a down-regulation of the m6A erasers *ALKBH5* and *FTO* [64]. In systemic lupus erythematosus, PBMC *ALKBH5* and *YTHDF2* are downregulated, a presentation that is correlated with several clinical characteristics [65]. The mechanistic underpinnings of m6A RNA methylation underscore its pivotal role in modulating the functions of immune cells, thereby orchestrating the immune microenvironment's dynamics. Notably, the conditional ablation of the m6A methyltransferases Mettl3 and Mettl14 markedly mitigates the progression of colitis in a murine T cell transfer model, highlighting m6A's regulatory potential in immune-mediated inflammatory responses. This effect is partially attributed to the m6A-mediated modulation of the suppressor of cytokine signaling (Socs) family genes, which are crucial for immediate early gene responses in $CD4^+$ T cells.The regulation of Socs gene expression by Mettl3 and Mettl14 is a key determinant of RNA stability, influencing the degradation rate of Socs mRNA. Elevated SOCS protein levels, resulting from m6A modification, act to dampen the JAK-STAT5 signaling cascade, effectively curtailing T cell proliferation and differentiation in response to IL-7 stimulation [19]. Knockout of *Alkbh5* also protects against colitis and experimental autoimmune encephalomyelitis models, an effect that is due to the upregulation of m6A modification of *Ifng* and *Cxcl2* in $CD4^+$ T cells, leading to reduced RNA stability and protein expression [14]. Mettl3's interaction with IGF2BP3 and YTHDF2 crucially influences the proliferation of germinal center B cells [66]. Beyond immune cells, the influence of m6A modification extends to stem and epithelial cells, integral components of the immune microenvironment. In human kidney epithelial cells, for instance, IGF2BP2 engagement with m6A-modified regions of *Cebpd* mRNA promotes its stability, enhancing the translation of pivotal proteins such as CCAAT/enhancer binding protein β/δ and lipocalin-2 [67]. These proteins play essential roles in the progression of autoantibody-induced glomerulonephritis, showcasing the diverse implications of m6A modification across cell types involved in autoimmune pathology.Given these mechanistic insights, it becomes evident that m6A modification exerts a profound influence on the immune microenvironment's dynamics, potentially contributing to the pathogenesis of autoimmune conditions such as SS.

In an effort to elucidate the complex interplay between m6A RNA methylation modifications and the immune microenvironment in Sjögren's syndrome, our study embarked on a rigorous bioinformatics exploration, leveraging expression profiles from public databases and proprietary sequencing data. Initial observations in peripheral blood samples from SS patients revealed a pronounced elevation in activated $CD4^+$ T cells and B cells compared to healthy controls, a trend mirrored in our labial gland sample analyses. This consistency underscores an overarching active immune response across both systemic and localized environments in SS, characterized by significant immune cell infiltration and activation. Diving deeper, our comparative analysis identified disparities in the expression levels of m6A regulators—encompassing writers, readers, and erasers—between SS patients and control samples. The key m6A regulators (*YTHDF3*, *RBM15*, *YTHDC2*, *YTHDF1*, *RBM15B*, *ELAVL1*, and *ALKBH5*) associated with SS were filtered by the random forest algorithm and the multivariate logistic regression analysis. Further, an intriguing correlation emerged between the levels of immune cell infiltration, particularly activated $CD4^+$ T cells, and the expression of m6A modulators, with a marked association observed with m6A writers and readers. Experimental validation using murine models substantiated these correlations; stimulation with anti-CD3/CD28 antibodies led to the significant upregulation of m6A regulators in $CD4^+$ T cells. Among these up-regulated genes, *Alkbh5* and *Ythdf1* were activated $CD4^+$ T cell-related genes that were related to SS diagnosis. METTL3 was found to influence $CD4^+$ T cell proliferation and differentiation via the IL-7/STAT5/SOCS signaling axis [19], while ALKBH5 modulated $CD4^+$ T cell-mediated inflammatory responses through the demethylation of CXCL2 and IFN-γ mRNA [14]. Conversely, the role of *YTHDF1* within $CD4^+$ T cells remains an open question. These findings provide valuable insights and open up avenues for further research on how m6A

modifications regulate the SS immune microenvironment.

Indeed, leveraging unsupervised clustering methods to analyze m6A modulators has emerged as a powerful tool to elucidate their regulatory roles within the complex landscape of the SS immune microenvironment. Unsupervised clustering can help identify distinct patterns or subgroups of m6A-modulated genes that are associated with specific immune cells profiles or functional pathways, revealing the intricate interplay between epigenetic regulation and gene expression in SS. Originally applied by Zhang et al. in the context of gastric cancer [32], unsupervised clustering has since been adopted to investigate a variety of diseases [68–70], uncovering pivotal insights into the epigenetic mechanisms underlying diverse pathologies. Employing this methodology, our study identified two distinct patterns of m6A methylation modifications based on the expression of 16 key m6A modulators. These patterns exhibited significant differences in m6A regulator expression and were characterized by distinct immune microenvironmental features. Pattern A was characterized by greater activated $CD4^+$ T cells, an enhanced TCR signaling pathway, and an up-regulation of multiple MHC class II molecules, which is similar to the early stages of SS. Correlation analyses with clinical characteristics further validated these findings, with Pattern A patients showing lower levels of serum IgG, anti-La/SSB, and anti-Ro/SSA antibodies compared to those in Pattern B. Similarly, ESSDAI scores followed this trend, reinforcing the hypothesis that m6A modification patterns may serve as indicators of disease progression in SS. Differentially expressed genes (DEGs) between the two m6A modification patterns were classified as m6A-related genes, providing a foundation for biological function predictions and the identification of m6A-related hub genes. These genes were predominantly associated with immune response mechanisms and the MAPK signaling pathway, a critical axis in T cell activation and signal transduction. Our findings align with previous research demonstrating abnormal activation of the TLR9-dependent p38/MAPK pathway in early-stage SS models, with inhibition of this pathway ameliorating symptoms [71,72]. Furthermore, activation of this pathway has been implicated in increased apoptosis in human salivary gland cells, a hallmark of SS pathology [62]. Additionally, two hub genes *COMMD8* and *SRP9* were screened by the WGCNA and topological analyses.

COMMD8, a key component of the Copper metabolism Murr 1 domain-containing protein family, plays a crucial role in modulating the proinflammatory NF-κB pathway. Through its interaction with the IκB-targeting ubiquitin ligase within the COMMD8/CCDC22 complex, COMMD8 facilitates the degradation of IκB, thereby activating the NF-κB pathway [73]. The COMMD8/COMMD3 complex can recruit GRK6 to the chemokine CXCR4 and induce further phosphorylation of CXCR4, thereby initiating the MAPK signaling pathway and promoting the migration of B cells and humoral immune responses [74]. Epigenetic regulation of COMMD8, involving long non-coding RNAs (lncRNAs) such as *MALAT1* and LINC00657, has been implicated in the survival and proliferation of non-small cell lung cancer cells by modulating miRNA interactions [75,76]. Similarly, the LncRNA *MNX1-AS1/miR-218-5p/COMMD8* pathway mediates the migration ability of hepatocellular carcinoma cells [77]. SRP9 is one of the components of the signal recognition particle (SRP) complex, whose main function is to transport proteins to the corresponding organelles [78]. Multiple case reports including polymyositis [79], systemic lupus erythematosus [80], and SS [81] have shown that autoantibodies targeting SRP are associated with disease progression. Ye et al. constructed a gene signature based on five genes including *SRP9* to calculate risk scores and predict relapse-free survival in patients with multiple sclerosis, suggesting that *SRP9* may play a regulatory function in this autoimmune disease [82]. These predicted hub genes remain to be validated by MeRIP-seq and cytology experiments.

This study represents the inaugural exploration of m6A RNA methylation modifications within the context of Sjögren's syndrome, unveiling a novel relationship between epigenetic alterations and the disease's immune microenvironment. By integrating extensive datasets from public repositories and our own sequencing efforts, we have begun to unravel the complex epigenetic landscape underpinning the hyper-activation and aberrant differentiation of pro-inflammatory immune cells in SS. These initial findings contribute significantly to our understanding of SS, offering a promising foundation upon which precision therapies could be developed. There are several limitations that should be acknowledged in our study. Firstly, despite our efforts to include as many eligible samples as possible, the overall sample size remained relatively small. The study consisted of 47 control samples and 165 samples from individuals with SS. This limited sample size may impact the generalizability of the findings and the statistical power of the analyses. Secondly, the proposed pathogenetic model remains hypothetical, as conclusive empirical evidence supporting each sequential step is currently lacking. Thirdly, while our study indicated elevated expression levels of *METTL3*, *ALKBH5*, and *YTHDF1* in $CD4^+$ T cells from SS patients compared to healthy donors, the functional implications of these findings necessitate deeper investigation. Additional experiments, such as functional assays and perturbation studies, would provide a more comprehensive understanding of the specific regulatory mechanisms and pathways through which these m6A regulators contribute to the pathogenesis of SS.

5. Conclusions

This study illuminates the role of m6A methylation in the immune microenvironment of Sjögren's syndrome, revealing a significant correlation between m6A regulators and immune cell infiltration. By mapping m6A modification patterns, our research offers novel insights into SS's pathogenesis and highlights potential targets for innovative immunotherapy strategies.

Ethics approval and consent to participate

The research adhered to the Declaration of Helsinki principles and received ethical approval from the Shanghai Ninth People's Hospital's Ethics Committee, affiliated to Shanghai Jiao Tong University School of Medicine (Approval IDs: SH9H-2019-T159-2 and SH9H-2021-TK69-1). All participants provided written informed consent.

Consent for publication

Not applicable.

Funding

This research was funded by the National Natural Science Foundation of China (Grants No. 82201086, 82170976, 82001064, 81970951); Yangfan program of Shanghai Science and Technology Committee (22YF1422100); China Postdoctoral Science Foundation (2022M722113); The Cross project of Ninth People's Hospital Affiliated to Shanghai Jiao Tong university School of Medicine (JYJC202126); Fundamental research program funding of Ninth People's Hospital affiliated to Shanghai Jiao Tong university School of Medicine (JYZZ132); The 17th undergraduate training program for innovation of Shanghai Jiao Tong University School of medicine (1723Y524); and the Shanghai Summit & Plateau Disciplines.

Data availability statement

All datasets utilized in this study are detailed in **Additional File 1**, which lists the corresponding data banks/repositories.

CRediT authorship contribution statement

Junhao Yin: Conceptualization, Formal analysis, Software, Writing – original draft, Writing – review & editing. **Jiayao Fu:** Conceptualization, Methodology. **Jiabao Xu:** Validation, Data curation. **Changyu Chen:** Data curation, Formal analysis. **Hanyi Zhu:** Investigation. **Baoli Wang:** Resources. **Chuangqi Yu:** Resources. **Xiujuan Yang:** Methodology, Project administration. **Ruiyu Cai:** Methodology, Project administration. **Mengyang Li:** Methodology, Project administration. **Kaihan Ji:** Methodology, Project administration. **Wanning Wu:** Methodology, Project administration. **Yijie Zhao:** Investigation. **Zhanglong Zheng:** Software, Validation. **Yiping Pu:** Resources. **Lingyan Zheng:** Conceptualization.

Declaration of competing interest

The authors declare the following financial interests/personal relationships which may be considered as potential competing interests: Lingyan Zheng, Jiayao Fu reports financial support was provided by National Natural Science Foundation of China. Jiayao Fu reports financial support was provided by Yangfan program of Shanghai Science and Technology Committee. Jiayao Fu reports financial support was provided by China Postdoctoral Science Foundation.

Acknowledgments

Functional enrichment analyses were conducted with Sangerbox tools, available at http://vip.sangerbox.com/, a complimentary online platform for data analysis. We extend our appreciation to EditSprings (https://www.editsprings.cn) for their professional language services.

Appendix A. Supplementary data

Supplementary data to this article can be found online at https://doi.org/10.1016/j.heliyon.2024.e28645.

References

[1] Y. Tang, T. Zhou, X. Yu, Z. Xue, N. Shen, The role of long non-coding RNAs in rheumatic diseases, Nat. Rev. Rheumatol. 13 (2017) 657–669.
[2] C.P. Mavragani, H.M. Moutsopoulos, Sjögren's syndrome, Annu Rev Pathol Mech Dis 9 (2014) 273–285.
[3] R.I. Fox, Sjögren's syndrome, Lancet 366 (2005) 321–331. Elsevier.
[4] A.S. Malladi, K.E. Sack, S.C. Shiboski, et al., Primary Sjögren's syndrome as a systemic disease: a study of participants enrolled in an international Sjögren's syndrome registry, Arthritis Care Res. 64 (2012) 911–918.
[5] G. Nocturne, X. Mariette, Advances in understanding the pathogenesis of primary Sjögren's syndrome, Nat. Rev. Rheumatol. 9 (2013) 544–556.
[6] E. Theander, L. Vasaitis, E. Baecklund, et al., Lymphoid organisation in labial salivary gland biopsies is a possible predictor for the development of malignant lymphoma in primary Sjögren's syndrome, Ann. Rheum. Dis. 70 (2011) 1363–1368.
[7] R. Desrosiers, K. Friderici, F. Rottman, Identification of methylated nucleosides in messenger RNA from Novikoff hepatoma cells, Proc Natl Acad Sci U S A 71 (1974) 3971–3975.
[8] Y. Wang, L. Li, J. Li, et al., The emerging role of m6A modification in regulating the immune system and autoimmune diseases, Front. Cell Dev. Biol. 9 (2021) 1–14.
[9] Q. Luo, B. Fu, L. Zhang, Y. Guo, Z. Huang, J. Li, Decreased peripheral blood ALKBH5 Correlates with markers of autoimmune response in systemic lupus erythematosus, Dis. Markers 2020 (2020).
[10] W. Shi, Y. Zheng, S. Luo, et al., METTL3 promotes activation and inflammation of FLSs through the NF-κB signaling pathway in rheumatoid arthritis, Front. Med. 8 (2021) 1–17.
[11] R hua Song, J. Zhao, C qun Gao, Q. Qin, J an Zhang, Inclusion of ALKBH5 as a candidate gene for the susceptibility of autoimmune thyroid disease, Adv. Med. Sci. 66 (2021) 351–358.

[12] Y. Yang, P.J. Hsu, Y.S. Chen, Y.G. Yang, Dynamic transcriptomic m6A decoration: writers, erasers, readers and functions in RNA metabolism, Cell Res. 28 (2018) 616–624.
[13] Z. Shulman, N. Stern-Ginossar, The RNA modification N 6-methyladenosine as a novel regulator of the immune system, Nat. Immunol. 21 (2020) 501–512.
[14] J. Zhou, X. Zhang, J. Hu, et al., M6A demethylase ALKBH5 controls CD4+T cell pathogenicity and promotes autoimmunity, Sci. Adv. 7 (2021) 1–14.
[15] X. Zhao, R. Dong, L. Zhang, et al., N6-methyladenosine-dependent modification of circGARS acts as a new player that promotes SLE progression through the NF-κB/A20 axis, Arthritis Res. Ther. 24 (2022) 37.
[16] J. Fu, H. Shi, B. Wang, et al., LncRNA PVT1 links Myc to glycolytic metabolism upon CD4+ T cell activation and Sjögren's syndrome-like autoimmune response, J. Autoimmun. 107 (2020) 102358.
[17] L. Ye, H. Shi, C. Yu, et al., LncRNA Neat1 positively regulates MAPK signaling and is involved in the pathogenesis of Sjögren's syndrome, Int. Immunopharm. 88 (2020) 106992.
[18] J. Fu, Y. Pu, B. Wang, et al., Pharmacological inhibition of Glutaminase 1 normalized the metabolic state and CD4+ T cell response in Sjogren's syndrome, J Immunol Res 2022 (2022), 1–13.
[19] H.-B. Li, J. Tong, S. Zhu, et al., m6A mRNA methylation controls T cell homeostasis by targeting the IL-7/STAT5/SOCS pathways, Nature 548 (2017) 338–342.
[20] J. Tong, G. Cao, T. Zhang, et al., m(6)A mRNA methylation sustains Treg suppressive functions, Cell Res. 28 (2018) 253–256.
[21] Y. Baştanlar, M. Ozuysal, Introduction to machine learning, Methods Mol. Biol. 1107 (2014) 105–128.
[22] C. Dai, B. Sun, R. Wang, J. Kang, The application of artificial intelligence and machine learning in Pituitary Adenomas, Front. Oncol. 11 (2021) 784819.
[23] S. Kolluri, J. Lin, R. Liu, Y. Zhang, W. Zhang, Machine learning and artificial intelligence in pharmaceutical research and development: a review, AAPS J. 24 (19) (2022).
[24] C.J. Lessard, H. Li, I. Adrianto, et al., Variants at multiple loci implicated in both innate and adaptive immune responses are associated with Sjögren's syndrome, Nat. Genet. 45 (2013) 1284–1292.
[25] R. Edgar, Gene Expression Omnibus: NCBI gene expression and hybridization array data repository, Nucleic Acids Res. 30 (2002) 207–210.
[26] S. Tasaki, K. Suzuki, A. Nishikawa, et al., Multiomic disease signatures converge to cytotoxic CD8 T cells in primary Sjögren's syndrome, Ann. Rheum. Dis. 76 (2017) 1458–1466.
[27] M.E. Ritchie, B. Phipson, D. Wu, Y. Hu, C.W. Law, W. Shi, G.K. Smyth, Limma powers differential expression analyses for RNA-sequencing and microarray studies, Nucleic Acids Res. 43 (2015) e47.
[28] J. Taminau, S. Meganck, C. Lazar, et al., Unlocking the potential of publicly available microarray data using inSilicoDb and inSilicoMerging R/Bioconductor packages, BMC Bioinf. 13 (2012) 335.
[29] J.T. Leek, W.E. Johnson, H.S. Parker, A.E. Jaffe, J.D. Storey, The sva package for removing batch effects and other unwanted variation in high-throughput experiments, Bioinformatics 28 (2012) 882–883.
[30] Y.-T. Chen, J.-Y. Shen, D.-P. Chen, et al., Identification of cross-talk between m(6)A and 5mC regulators associated with onco-immunogenic features and prognosis across 33 cancer types, J. Hematol. Oncol. 13 (2020) 22.
[31] Y. Li, J. Xiao, J. Bai, et al., Molecular characterization and clinical relevance of m(6)A regulators across 33 cancer types, Mol. Cancer 18 (2019) 137.
[32] B. Zhang, Q. Wu, B. Li, D. Wang, L. Wang, Y.L. Zhou, m(6)A regulator-mediated methylation modification patterns and tumor microenvironment infiltration characterization in gastric cancer, Mol. Cancer 19 (2020) 53.
[33] F. Ye, T. Wang, X. Wu, J. Liang, J. Li, W. Sheng, N6-Methyladenosine RNA modification in cerebrospinal fluid as a novel potential diagnostic biomarker for progressive multiple sclerosis, J. Transl. Med. 19 (2021) 1–14.
[34] F. Li, Y. Zhang, Z. Peng, Y. Wang, Z. Zeng, Z. Tang, Diagnostic, clustering, and immune cell infiltration analysis of m6A regulators in patients with sepsis, Sci. Rep. 13 (2023) 1–11.
[35] Z. Jin, J. Shang, Q. Zhu, C. Ling, W. Xie, B. Qiang, RFRSF: employee turnover prediction based on random forests and survival analysis, Lect Notes Comput Sci (including Subser Lect Notes Artif Intell Lect Notes Bioinformatics) 12343 LNCS (2020) 503–515.
[36] A. Karatzoglou, A. Smola, K. Hornik, A. Zeileis, Kernlab - an S4 package for kernel methods in R, J Stat Softw 11 (2004) 1–20.
[37] X. Robin, N. Turck, A. Hainard, N. Tiberti, F. Lisacek, J.-C. Sanchez, M. Müller, pROC: an open-source package for R and S+ to analyze and compare ROC curves, BMC Bioinf. 12 (2011) 77.
[38] P. Biecek, Dalex: explainers for complex predictive models in R, J. Mach. Learn. Res. 19 (2018) 1–5.
[39] M.D. Wilkerson, D.N. Hayes, ConsensusClusterPlus: a class discovery tool with confidence assessments and item tracking, Bioinformatics 26 (2010) 1572–1573.
[40] D.A. Barbie, P. Tamayo, J.S. Boehm, et al., Systematic RNA interference reveals that oncogenic KRAS-driven cancers require TBK1, Nature 462 (2009) 108–112.
[41] S. Hänzelmann, R. Castelo, J. Guinney, GSVA: gene set variation analysis for microarray and RNA-seq data, BMC Bioinf. 14 (7) (2013).
[42] S. Bhattacharya, S. Andorf, L. Gomes, et al., ImmPort: disseminating data to the public for the future of immunology, Immunol. Res. 58 (2014) 234–239.
[43] S. Tweedie, B. Braschi, K. Gray, T.E.M. Jones, R.L. Seal, B. Yates, E.A. Bruford, Genenames.org: the HGNC and VGNC resources in 2021, Nucleic Acids Res. 49 (2021) D939–D946.
[44] R. Seror, P. Ravaud, S.J. Bowman, et al., EULAR Sjögren's syndrome disease activity index: development of a consensus systemic disease activity index for primary Sjögren's syndrome, Ann. Rheum. Dis. 69 (2010) 1103–1109.
[45] J. Yin, X. Zeng, Z. Ai, M. Yu, Y. Wu, S. Li, Construction and analysis of a lncRNA-miRNA-mRNA network based on competitive endogenous RNA reveal functional lncRNAs in oral cancer, BMC Med Genomics 13 (2020) 1–14.
[46] J. Yin, Z. Zheng, X. Zeng, et al., lncRNA MALAT1 mediates osteogenic differentiation of bone mesenchymal stem cells by sponging miR-129-5p, PeerJ 10 (2022) e13355.
[47] T. Wu, E. Hu, S. Xu, et al., clusterProfiler 4.0: a universal enrichment tool for interpreting omics data, Innov 2 (2021) 100141. Cambridge.
[48] J. Tang, D. Kong, Q. Cui, K. Wang, D. Zhang, Y. Gong, G. Wu, Prognostic genes of breast cancer identified by gene Co-expression network analysis, Front. Oncol. 8 (2018) 374.
[49] Ø. Bruserud, Effects of azoles on human acute myelogenous leukemia blasts and T lymphocytes derived from acute leukemia patients with chemotherapy-induced cytopenia, Int. Immunopharm. 1 (2001) 2183–2195.
[50] Guide for the Care and Use of Laboratory Animals, National Academies Press, Washington, D.C., Washington (DC), 2011.
[51] D. Yu, J.R. Horton, J. Yang, et al., Human MettL3-MettL14 RNA adenine methyltransferase complex is active on double-stranded DNA containing lesions, Nucleic Acids Res. 49 (2021) 11629–11642.
[52] Q. Wang, X. Guo, L. Li, Z. Gao, X. Su, M. Ji, J. Liu, N6-methyladenosine METTL3 promotes cervical cancer tumorigenesis and Warburg effect through YTHDF1/HK2 modification, Cell Death Dis. 11 (2020) 911.
[53] H. Li, H. Wu, W. Li, J. Zhou, J. Yang, W. Peng, Constructing a multiple sclerosis diagnosis model based on microarray, Front. Neurol. 12 (2022) 1–10.
[54] J. Fu, H. Shi, B. Wang, et al., LncRNA PVT1 links Myc to glycolytic metabolism upon CD4+ T cell activation and Sjögren's syndrome-like autoimmune response, J. Autoimmun. 107 (2020) 102358.
[55] Y. Shao, J. Fu, T. Zhan, L. Ye, C. Yu, Fangchinoline inhibited proliferation of neoplastic B-lymphoid cells and alleviated Sjögren's syndrome-like responses in NOD/Ltj mice via the Akt/mTOR pathway, Curr. Mol. Pharmacol. 31 (2022) 2431–2443.
[56] T. Zhan, B. Wang, J. Fu, Y. Shao, L. Ye, H. Shi, L. Zheng, Artesunate inhibits Sjögren's syndrome-like autoimmune responses and BAFF-induced B cell hyperactivation via TRAF6-mediated NF-κB signaling, Phytomedicine 80 (2021) 153381.
[57] J.M. Van Woerkom, A.A. Kruize, M.J.G. Wenting-Van Wijk, et al., Salivary gland and peripheral blood T helper 1 and 2 cell activity in Sjögren's syndrome compared with non-Sjögren's sicca syndrome, Ann. Rheum. Dis. 64 (2005) 1474–1479.
[58] H. Shi, N. Cao, Y. Pu, L. Xie, L. Zheng, C. Yu, Long non-coding RNA expression profile in minor salivary gland of primary Sjögren's syndrome, Arthritis Res. Ther. 18 (2016) 109.
[59] J. Yin, J. Fu, Y. Shao, et al., CYP51-mediated cholesterol biosynthesis is required for the proliferation of CD4+ T cells in Sjogren's syndrome, Clin. Exp. Med. 23 (2022) 1691–1711.

[60] J.J. Letterio, A.G. Geiser, A.B. Kulkarni, et al., Autoimmunity associated with TGF-β1-deficiency in mice is dependent on MHC class II antigen expression, J. Clin. Invest. 98 (1996) 2109–2119.
[61] X. Chen, P. Zhang, Q. Liu, et al., Alleviating effect of paeoniflorin-6'-O-benzene sulfonate in antigen-induced experimental Sjögren's syndrome by modulating B lymphocyte migration via CXCR5-GRK2-ERK/p38 signaling pathway, Int. Immunopharm. 80 (2020) 106199.
[62] J. Fu, H. Shi, N. Cao, et al., Toll-like receptor 9 signaling promotes autophagy and apoptosis via divergent functions of the p38/JNK pathway in human salivary gland cells, Exp. Cell Res. 375 (2019) 51–59.
[63] P. Shannon, A. Markiel, O. Ozier, et al., Cytoscape: a software Environment for integrated models of biomolecular interaction networks, Genome Res. 13 (2003) 2498–2504.
[64] Q. Luo, Y. Gao, L. Zhang, J. Rao, Y. Guo, Z. Huang, J. Li, Decreased ALKBH5, FTO, and YTHDF2 in peripheral blood are as risk factors for rheumatoid arthritis, BioMed Res. Int. 2020 (2020).
[65] Q. Luo, J. Rao, L. Zhang, B. Fu, Y. Guo, Z. Huang, J. Li, The study of METTL14, ALKBH5, and YTHDF2 in peripheral blood mononuclear cells from systemic lupus erythematosus, Mol Genet Genomic Med 8 (2020) 1–10.
[66] A.C. Grenov, L. Moss, S. Edelheit, et al., The germinal center reaction depends on RNA methylation and divergent functions of specific methyl readers, J. Exp. Med. 218 (2021).
[67] R. Bechara, N. Amatya, R.D. Bailey, et al., The m6A reader IMP2 directs autoimmune inflammation through an IL-17 and TNFα-dependent C/EBP transcription factor axis, Sci Immunol 6 (2021).
[68] Y. Fan, Y. Zhou, M. Lou, X. Li, X. Zhu, K. Yuan, m6A regulator-mediated methylation modification patterns and characterisation of tumour microenvironment infiltration in non-small cell lung cancer, J. Inflamm. Res. 15 (2022) 1969–1989.
[69] H. Zhao, S. Pan, J. Duan, F. Liu, G. Li, D. Liu, Z. Liu, Integrative analysis of m6A regulator-mediated RNA methylation modification patterns and immune characteristics in lupus nephritis, Front. Cell Dev. Biol. 9 (2021) 1–16.
[70] X. Zhang, S. Zhang, X. Yan, et al., m6A regulator-mediated RNA methylation modification patterns are involved in immune microenvironment regulation of periodontitis, J. Cell Mol. Med. 25 (2021) 3634–3645.
[71] H. Shi, C.-Q. Yu, L.-S. Xie, Z.-J. Wang, P. Zhang, L.-Y. Zheng, Activation of TLR9-dependent p38MAPK pathway in the pathogenesis of primary Sjögren's syndrome in NOD/Ltj mouse, J oral Pathol Med Off Publ Int Assoc Oral Pathol Am Acad Oral Pathol 43 (2014) 785–791.
[72] N. Cao, H. Shi, C. Chen, L. Zheng, C. Yu, Inhibition of the TLR9-dependent p38 MAPK signaling pathway improves the pathogenesis of primary Sjögren's syndrome in the NOD/Ltj mouse, J. Biol. Regul. Homeost. Agents 35 (2021) 1103–1108.
[73] P. Starokadomskyy, N. Gluck, H. Li, et al., CCDC22 deficiency in humans blunts activation of proinfammatory NF-κB signaling, J. Clin. Invest. 123 (2013) 2244–2256.
[74] A. Nakai, J. Fujimoto, H. Miyata, et al., The COMMD3/8 complex determines GRK6 specificity for chemoattractant receptors, J. Exp. Med. 216 (2019) 1630–1647.
[75] S. Wang, T. Wang, D. Liu, H. Kong, LncRNA MALAT1 aggravates the progression of non-small cell lung cancer by stimulating the expression of COMMD8 via targeting miR-613, Cancer Manag. Res. 12 (2020) 10735–10747.
[76] R. Zhang, Z. Niu, H. Pei, Z. Peng, Long noncoding RNA LINC00657 induced by SP1 contributes to the non-small cell lung cancer progression through targeting miR-26b-5p/COMMD8 axis, J. Cell. Physiol. 235 (2020) 3340–3349.
[77] D. Ji, Y. Wang, B. Sun, J. Yang, X. Luo, Long non-coding RNA MNX1-AS1 promotes hepatocellular carcinoma proliferation and invasion through targeting miR-218-5p/COMMD8 axis, Biochem. Biophys. Res. Commun. 513 (2019) 669–674.
[78] M. Halic, R. Beckmann, The signal recognition particle and its interactions during protein targeting, Curr. Opin. Struct. Biol. 15 (2005) 116–125.
[79] T. Miller, M.T. Al-Lozi, G. Lopate, A. Pestronk, Myopathy with antibodies to the signal recognition particle: clinical and pathological features, J. Neurol. Neurosurg. Psychiatry 73 (2002) 420–428.
[80] G.J.D. Hengstman, H.J. ter Laak, W.T.M. Vree Egberts, et al., Anti-signal recognition particle autoantibodies: marker of a necrotising myopathy, Ann. Rheum. Dis. 65 (2006) 1635–1638.
[81] N. Takahashi, A. Nishida, J. Tsugawa, M. Okajima, S. Fujioka, Y. Tsuboi, [A case of immune-mediated necrotizing myopathy associated with primary sjögren syndrome], Brain Nerve 73 (2021) 183–187.
[82] F. Ye, J. Liang, J. Li, H. Li, W. Sheng, Development and validation of a five-gene signature to predict relapse-free survival in multiple sclerosis, Front. Neurol. 11 (2020) 1–12.